IEEE Open Journal of the Communications Society

Received 29 July 2026; accepted 14 September 2026. Date of publication 22 September 2026; date of current version 2 October 2026.

Digital Object Identifier 10.1109/OJCOMS.2026.3736258

AFDM: Evolving OFDM Toward 6G+

HYEON SEOK ROU[1] (Member, IEEE), VINCENT SAVAUX[2] (Senior Member, IEEE), ZEPING SUI[3] (Member, IEEE), GIUSEPPE THADEU FREITAS DE ABREU[1] (Senior Member, IEEE), AND ZILONG LIU[3] (Senior Member, IEEE)

[1]School of Computer Science and Engineering, Constructor University Bremen, 28759 Bremen, Germany
[2]Institute of Research and Technology b-com, 35510 Cesson Sévigné, France
[3]School of Computer Science and Electronics Engineering, University of Essex, CO4 3SQ Colchester, U.K.

CORRESPONDING AUTHOR: H. S. ROU (hsrou@ieee.org)

The work of Zilong Liu was supported in part by U.K. Engineering and Physical Sciences Research Council under Grant EP/Y037243/1 ('TITAN/REVOL6G' and 'TITAN/LEGEND6G'), Grant EP/X040569/1 ('HASC/RETHIN6G'), Grant EP/X035352/1 ('DRIVE'), and Grant EP/Y000986/1 ('SORT'); and in part by the Royal Society under Grant IECNSFC233292 and Grant IESR1241212.

ABSTRACT As sixth generation (6G) standardization accelerates, there is growing consensus in favor of *evolutionary* waveforms that add new capabilities while preserving compatibility with the orthogonal frequency division multiplexing (OFDM) core of 4G and 5G. This article positions affine frequency division multiplexing (AFDM) as such a candidate, providing structural robustness for high-mobility communications and integrated sensing and communication (ISAC) over doubly dispersive channels while remaining backward-compatible with the legacy OFDM air interface. We first develop a generalized fractional-delay-fractional-Doppler (FDFD) channel model that accounts for practical pulse-shaping filters and the resulting inter-sample coupling. Building on this model, we show that the AFDM transceiver reuses nearly the entire OFDM chain, adding only lightweight digital pre- and post-processing. We then analyze the impact of hardware impairments such as phase noise and carrier frequency offset, and examine the advanced functionalities enabled by the chirp-parameter domain, including index modulation and physical-layer security. Assessing reusability across the radio-frequency, physical, and higher layers, we conclude that AFDM offers an efficient path toward high-fidelity later versions of 6G and beyond (6G$\mathcal{C}$) communications.

INDEX TERMS Affine frequency division multiplexing (AFDM), orthogonal frequency division multiplexing (OFDM), evolutionary, 6G and beyond (6G+), backward compatibility, system reusability.

I. INTRODUCTION

A. BACKGROUND

IT IS widely anticipated that sixth generation (6G) systems will bring substantial advances across both technological and application domains, beyond the incremental gains realized in the transition from fourth generation (4G) to fifth generation (5G) systems [1], [2]. Besides the development of new 6G use cases, such as the integration of artificial intelligence (AI) technology and integrated sensing and communication (ISAC) functionalities, this evolution will also be shaped by recent decisions [3], [4], [5] reached by 3GPP, reaffirming the use of orthogonal frequency division multiplexing (OFDM), specifically cyclic prefix orthogonal frequency division multiplexing (CP-OFDM) and discrete Fourier transform spread orthogonal frequency division multiplexing (DFT-s-OFDM), as the baseline waveform for 6G [6], [7], [8]. This choice was motivated by the maturity of OFDM technology, which has been extensively deployed and refined across multiple wireless systems. A wide range of techniques such as peak-to-average power ratio (PAPR) reduction [9], carrier frequency offset (CFO) calibration [10], and advanced channel estimation and tracking methods [11], [12], have been developed and proven effective in mitigating inherent limitations of OFDM, further strengthening it as a solid foundation for the sixth generation (6G) air interface design [13].

However, this decision should not be taken to mean that the 6G waveform is finalized. In fact, 3GPP leaves the door open for investigating new waveforms designed to address the limitations of OFDM in future 6G use cases and to facilitate the integration of multiple functionalities, such as sensing and computing.

Candidate waveform solutions for later versions of 6G and beyond (6G+) must remain closely aligned with the OFDM legacy, emphasizing backward compatibility, coexistence, and hardware reusability [3]. This creates a stringent requirement: any 6G+ waveform must reuse the existing OFDM infrastructure as much as possible while address-

© 2026 The Authors. This work is licensed under a Creative Commons Attribution 4.0 License.
For more information, see https://creativecommons.org/licenses/by/4.0/

ing challenges that conventional OFDM cannot overcome. Firstly, next-generation waveforms must cope with the deteriorating effects of high-mobility channels [14] and/or high-frequency bands (e.g., millimeter wave or Terahertz), which generally suffer from large path loss and strong phase noise and/or carrier frequency offsets. Secondly, next-generation waveforms are expected to offer improved sensing capabilities compared to OFDM counterparts [15].

These requirements are central to the evolution envisioned for 6G+. For example, non-terrestrial networks (NTN) scenarios, consisting of satellite systems, high-altitude platform station (HAPS), and flying drones [16], are characterized by high moving speeds that induce Doppler shifts/spread far beyond the tolerance of OFDM, even under advanced mitigation strategies. Similarly, in direct device-to-device (D2D) and sidelink communications, which are expected to play a central role in 6G for applications such as vehicle-to-vehicle (V2V) and vehicle-to-everything (V2X), or drone-to-drone connectivity [17], the non-stationary mobile channels and the lack of centralized synchronization further expose the vulnerability of OFDM to Doppler impairments [18].

An additional dimension arises with ISAC, whose demand is widely present in the aforementioned scenarios [19]. In ISAC systems, the waveform must not only support reliable data transmission but also enable accurate estimation of the range and velocity for effective environment sensing [20]. In a highly dynamic 6G system, such a requirement may not be fulfilled by OFDM as it lacks the intrinsic robustness to joint delay-Doppler variations.

B. WHY AFDM?

In the context of the above, it is clear that a new waveform paradigm is needed to truly enable 6G to its full extent, one that simultaneously preserves OFDM's efficiency advantages while embracing, rather than counteracting, the characteristics of doubly dispersive channels.

To this end, affine frequency division multiplexing (AFDM) [21] has emerged recently as one of the waveform paradigms proposed for this purpose. Unlike conventional OFDM, which modulates each information symbol onto a separate orthogonal subcarrier, AFDM employs chirp-based subcarriers whose instantaneous frequencies increase linearly over time. With the affine Fourier transform (AFT), AFDM spreads each symbol across the time and frequency domains, thereby enjoying the full channel diversity as well as strong resilience to Doppler (an intrinsic property of chirps).

In addition, the chirp parameters of AFDM are tunable, enabling flexible adaptation to the characteristics of the channel to ensure maximum diversity for optimal communications performance over a variety of channel settings [22], [23], in addition to the ability to support advanced functionalities such as index modulation [24], [25], [26], [27], [28] and physical-layer security [29], [30], [31]. In light of these advantages of the affine frequency domain, AFDM has also motivated in various derivative and related schemes exploiting the chirp-based waveform structure [32], [33], [34], [35], [36].

Furthermore, from hardware implementation perspective, AFDM can be regarded as a direct extension and generalization of OFDM, where the latter is reduced to AFDM under specific parameter settings [22]. Namely, the transceiver processing chain of AFDM remains largely intact, with only an additional linear-complexity pre- and post-processing step applied around the conventional inverse fast Fourier transform (IFFT)/fast Fourier transform (FFT) operations of OFDM. Consequently, AFDM is inherently compatible to OFDM, allowing the reuse of key signal processing blocks such as IFFT/FFT modules, parallel-to-serial conversion, time-frequency resource management, and prefix handling. Moreover, the extensive body of OFDM enhancements, including PAPR reduction, pulse shaping, and spectral containment methods, can be applied to AFDM with only minor adaptation, given the fundamental similarity in signal structure across time-frequency subcarriers.

On the other hand, competing waveform proposals such as orthogonal time-frequency space (OTFS) [37], orthogonal time-sequency multiplexing (OTSM) [38], orthogonal delay-Doppler multiplexing (ODDM) [39], and Zak-OTFS [40] adopt a distinct signaling framework. Instead of operating in the time-frequency domain, as that in OFDM and AFDM, these schemes modulate the information symbols onto the two-dimensional delay-Doppler domain [41], [42], with the aim to exploit the inherent delay-Doppler sparsity of doubly dispersive channels [14]. As a result, they have been shown to also achieve strong theoretical performance in high-mobility scenarios [43], [44].

However, such performance comes at the cost of additional system-level modifications relative to OFDM, including different resource allocation approaches, domain transforms, and dimensions, as well as modified multiple access schemes, particularly under practical pulse-shaping conditions. FFT-based simplified implementations of OTFS (e.g., under rectangular pulse shaping) can reuse parts of the OFDM processing chain, but full pulse-shaped implementations require 2D processing. Consequently, their integration into existing OFDM-dominated architectures would require additional modifications at both the physical and higher layers, thereby reducing compatibility [22].

This requirement specifically runs counter to recent standardization decisions favoring OFDM-based evolution and therefore complicates the adoption of such schemes within the current OFDM-based evolutionary roadmap.

C. CONTRIBUTIONS OF THIS ARTICLE

A major objective of this article is to analyze AFDM as a candidate for next-generation air interfaces, capable of addressing the requirements of 6G, including extreme mobility, NTN operation, D2D communications, ISAC, and PHY-security, while preserving architectural compatibility with the OFDM legacy.

Going beyond the current state-of-the-art of AFDM, reviewing its reported performance advantages over OFDM in challenging 6G channel conditions and various use cases [20], [21], [45], [46], [47], [48], [49], [50], [51], [52], [53], [54], this article provides a comprehensive analysis of AFDM from a practical implementation perspective. Specifically, we examine its feasibility in direct comparison with OFDM across several critical dimensions:

- Compatibility of AFDM with OFDM hardware and signal processing blocks, reusing existing OFDM modules such as FFT, pulse shaping, prefixing, and resource management.
- Implementation complexity and overhead of AFDM compared to OFDM, in aspects such as transceiver processing, channel estimation, and detection.
- Robustness of AFDM in the presence of the challenging fractional-delay-fractional-Doppler (FDFD) conditions, channel estimation errors, and hardware impairments.
- Advanced functionalities enabled by AFDM, such as multiple access and coexistence with OFDM, chirp-domain modulation, and physical-layer security.

Finally, we qualitatively evaluate the reusability of AFDM across the radio frequency (RF), physical layer (PHY), and higher layers, against the legacy OFDM, indicating its potential for smooth and evolutionary integration into 6G+.

D. ORGANIZATION OF THIS ARTICLE

The remainder of this article is structured as follows: Section II introduces the system and channel models adopted throughout the article, including a novel general FDFD channel input-output model based on physical pulse footprints that accurately captures inter-sample coupling in practical transceiver implementations; Section III details the transceiver architecture of AFDM, highlighting its compatibility and reusability with respect to OFDM, considering various aspects, such as prefixing, pulse shaping, and resource management; Section IV presents a variety of thorough analyses of AFDM in comparison with OFDM, including implementation complexity and scalability, channel estimation and detection architecture, robustness to impairments like phase noise (PHN) and CFO, and advanced functionalities including multiple-input multiple-output (MIMO), chirp-domain modulation and physical-layer security; Section IV additionally concludes with a qualitative, layer-wise summary of the reusability of AFDM compared with legacy OFDM; Section V then outlines the open research challenges and future directions, including synchronization and standardization pathways, as well as the concluding remarks.

Notation: Scalars, vectors, and matrices are denoted by lowercase, bold lowercase, and bold uppercase letters, respectively, e.g., x, $\mathbf{x}$, and $\mathbf{X}$. The i-th element of a vector $\mathbf{x}$ is denoted by x_i, and the (i,j)-th element of a matrix $\mathbf{X}$ by $x_{i,j}$. When subscripts become overly dense, the alternative notations $[\mathbf{x}]_i$ and $[\mathbf{X}]_{i,j}$ may be used for clarity. The transpose, Hermitian transpose, and inverse of a matrix $\mathbf{X}$ are denoted by $\mathbf{X}^{\mathsf{T}}$, $\mathbf{X}^{\mathsf{H}}$, and $\mathbf{X}^{-1}$, respectively. The operators $\otimes$ and $\odot$ respectively denote the Kronecker and Hadamard product, and $*$ the linear convolution. The sets of natural, integer, rational, real, and complex numbers are denoted by $\mathbb{N}$, $\mathbb{Z}$, $\mathbb{Q}$, $\mathbb{R}$, and $\mathbb{C}$, respectively. $\delta(\cdot)$ represents the Dirac delta function, while $\delta[\cdot]$ denotes the Kronecker delta. The modulo-N operation is denoted by $(\cdot)_N$.

II. SYSTEM MODEL

We first present the continuous-time single-input single-output (SISO) doubly dispersive channel model and its corresponding discrete-time equivalent representation, leading to the general fractional-delay-fractional-Doppler (FDFD) input-output relation in matrix form, which will be used throughout this article. We note that the continuous- and discrete-time channel models and the integer-delay-integer-Doppler (IDID)/integer-delay-fractional-Doppler (IDFD) special cases are standard background. The generalized FDFD matrix decomposition of Section II-C explicitly incorporates the transmit pulse-shaping kernel. To the best of our knowledge, our generalized FDFD case is a novel contribution (see Remark 1).

A. CONTINUOUS-TIME SISO DOUBLY DISPERSIVE CHANNEL

Consider a wireless channel with P resolvable scattering propagation paths, characterized by its continuous-time time-varying impulse response function (TVIRF) given by [14]

$$h(t,\tau) = \sum_{p=1}^{P} h_p\, e^{j2\pi\nu_p t}\, \delta(\tau-\tau_p), \tag{1}$$

where $h_p \in \mathbb{C}$ denotes the complex gain, $\tau_p \in \mathbb{R}$ denotes the propagation delay, and $\nu_p \in \mathbb{R}$ denotes the associated Doppler frequency shift of the p-th path, and the combined influence of the path delays τ_p (frequency selectivity) and Doppler shifts ν_p (time selectivity) gives rise to the so-called doubly dispersive fading environment.

The maximum delay spread and maximum Doppler spread of the channel are defined as $\tau_{\max} \in \mathbb{R}^+$ and $\nu_{\max} \in \mathbb{R}^+$, respectively, such that $\tau_p \in [0, \tau_{\max}]$ and $\nu_p \in [-\nu_{\max}, \nu_{\max}]$ for $p \in \{1,\dots,P\}$, and the channel is considered underspread if $\tau_{\max}\nu_{\max} \ll 1$, and overspread otherwise.

Then, given an arbitrary time-domain transmit signal $s(t)$, the corresponding input-output relation in the continuous-time domain is given by a linear convolution with the TVIRF in (1), which is expressed as

$$r(t) = s(t) * h(t,\tau) + w(t) = \int_{-\infty}^{+\infty} h(t,\tau)s(t-\tau)\,d\tau + w(t), \tag{2}$$

where $r(t)$ and $w(t)$ represent the time-domain received signal over the doubly dispersive channel and the additive white Gaussian noise (AWGN) signal, respectively.

B. DISCRETE-TIME EQUIVALENT MODEL

To represent the continuous system model in a manner compatible with discrete signal processing, the

continuous-time signal is sampled at a sampling interval of $T_s \triangleq \frac{1}{f_s}$, where f_s is the sampling frequency in Hz.

Then, denoting $n \in \{0, \ldots, N-1\}$ as the sample index of the discrete sequence, the discrete-time channel input-output relation is expressed as

$$r[n] = \sum_{p=1}^{P} h_p \, e^{j2\pi \nu_p n T_s} \, s\left[n - \frac{\tau_p}{T_s}\right] + w[n], \tag{3}$$

where $r[n]$, $s[n]$, and $w[n]$ are the sampled received, transmitted, and noise signal sequences, respectively.

Then, defining the normalized delay indices and the normalized digital Doppler shift indices as

$$\ell_p \triangleq \frac{\tau_p}{T_s}, \; f_p \triangleq N \nu_p T_s = N \frac{\nu_p}{f_s}, \tag{4}$$

where N is the total number of samples in the sequence, the discrete-time input-output relation in (3) can be rewritten as

$$r[n] = \sum_{p=1}^{P} h_p \, e^{j2\pi f_p \frac{n}{N}} \, s[n - \ell_p] + w[n]. \tag{5}$$

Notice that the delay index ℓ_p represents the physical delay (in seconds) normalized by the sampling interval T_s, while the digital Doppler shift index f_p represents the physical Doppler shift (in Hz) normalized by the subcarrier spacing $\frac{f_s}{N}$. Therefore, depending on the channel scenario (i.e., the delay-Doppler profile) and the sampling frequency, the normalized indices ℓ_p and f_p may take either integer or fractional values, categorized into the following three cases:

1) CASE 1: INTEGER DELAY AND INTEGER DOPPLER (IDID)

When both the normalized path delays and digital Doppler shifts are integer-valued, *i.e.*, $\ell_p \in \mathbb{Z}_{\geq 0}$ and $f_p \in \mathbb{Z}$, the multipath components are perfectly aligned with the discrete sampling and frequency grids. For this case, here onwards referred to as IDID channel, the discrete-time baseband received signal can be described by (5) directly without concern as ℓ_p is an integer, and therefore the shifted samples $s[n - \ell_p]$ are well-defined. Furthermore, the phase rotation term $e^{j2\pi f_p \frac{n}{N}}$ is an integer multiple of $e^{\frac{j2\pi}{N}}$, which corresponds to the fundamental frequency resolution of the discrete Fourier basis.

This is a common assumption adopted in most existing works, as it greatly simplifies the analysis and design of communication systems, reveals the core characteristics and behavior of each delay-Doppler tap without interference or added complexity. However, such an assumption is often unrealistic in practical scenarios, where the delay and Doppler parameters are typically not perfectly aligned with the discrete grids, especially the Doppler shifts, necessitating more general models.

2) CASE 2: INTEGER DELAY AND FRACTIONAL DOPPLER (IDFD)

In the IDFD case, the assumption of integer Doppler shifts is relaxed to reflect practical high-mobility environments better. Here, the normalized path delays remain integer-valued while the digital Doppler shifts are allowed to take non-integer (fractional) values, *i.e.*, $\ell_p \in \mathbb{Z}_{\geq 0}$ and $f_p \in \mathbb{R}$. Note that the assumption of integer delays remains relatively robust, as the high sampling rate f_s provides a sufficiently fine resolution T_s to align multipath arrivals with the discrete, integer-indexed grid.

In this case, the discrete-time model retains the structural form of (5), as the integer-shifted samples $s[n - \ell_p]$ are still aligned with the sampling instances. However, a critical distinction emerges in the phase rotation term $e^{j2\pi f_p \frac{n}{N}}$, where the Doppler shifts no longer correspond to integer multiples of the fundamental frequency resolution $e^{\frac{j2\pi}{N}}$. This misalignment breaks the periodic orthogonality of the discrete Fourier basis, the cornerstone of legacy waveforms such as OFDM, thereby introducing significant inter-carrier interference (ICI) and spectral leakage.

3) CASE 3: FRACTIONAL DELAY AND FRACTIONAL DOPPLER (FDFD)

Finally, the FDFD model represents the most generalized and physically accurate case, where both the normalized delays and digital Doppler frequencies take arbitrary real values, *i.e.*, $\ell_p \in \mathbb{R}_{\geq 0}$ and $f_p \in \mathbb{R}$. While integer delays are often acceptable in systems with moderate delays, fractional delays may become significant in ultra-high-precision synchronization and sensing applications.

In this case, the time-shifted argument $(n - \ell_p)$ in the transmit sequence is no longer strictly integer-valued. Consequently, the term $s[n - \ell_p]$ cannot be obtained by a simple index shift as in (5). This *fractionally delayed* version of the discrete sequence physically corresponds to the continuous-time signal being reconstructed from the discrete samples via a convolutional pulse-shaping filter $p(t)$, shifted by the continuous delay τ_p, and subsequently resampled at the receiver's sampling grid.

This process is mathematically expressed through a discrete-time interpolation, given by

$$s[n - \ell_p] = \sum_{m=0}^{N-1} s[m] \, g\big((n - m) - \ell_p\big), \tag{6}$$

where $g(\cdot)$ denotes the effective discrete-time pulse kernel, derived from the underlying pulse-shaping filter $p(t)$ such that $g(m) = p(mT_s)$, with sampling interval T_s.

Note that unlike idealized digital interpolation (e.g., sinc-based upsampling), which is independent of the waveform, the kernel $g(\cdot)$ in this model reflects the actual hardware pulse footprint (e.g., raised cosine or rectangular).

Then, by substituting (6) into the discrete-time input-output relation in (3), we obtain the expanded discrete-time representation for a FDFD channel as

$$r[n] = \sum_{p=1}^{P} h_p \, e^{j2\pi f_p \frac{n}{N}} \sum_{m=0}^{N-1} s[m] \, g\big((n - m) - \ell_p\big) + w[n]. \tag{7}$$

This formulation reveals that the choice of the physical pulse shape $p(t)$ directly governs the inter-sample coupling

in the discrete domain. Consequently, this model provides a high-fidelity foundation that simultaneously accounts for spectral leakage due to fractional Doppler and the inter-sample interference caused by fractional delays, which is essential for evaluating next-generation waveforms in 6G propagation environments.

C. GENERALIZED MATRIX-FORM INPUT-OUTPUT RELATIONSHIP

To facilitate efficient and insightful analysis, the discrete-time input-output relation for the FDFD channel in (7) can be equivalently expressed using a matrix-vector formulation. Namely, given a transmitted symbol block $\mathbf{s} \in \mathbb{C}^{N\times 1}$ of N samples, the received vector $\mathbf{r} \in \mathbb{C}^{N\times 1}$ is obtained under a circular convolution framework with a general prefix.

The signal sequence $s[n]$ is prepended with a prefix of length N_{cp}, described by

$$s[n'] = s[N+n'] \cdot e^{j2\pi\phi_{\text{cp}}(n')}, \ \forall n' \in \{-N_{\text{cp}}, \ldots, -1\}, \tag{8}$$

where $\phi_{\text{cp}}(\cdot)$ is the waveform-dependent phase-offset function of the prefix samples, elaborated in Section III.

Given the above, the overall convolution matrix $\mathbf{H} \in \mathbb{C}^{N\times N}$ represents the doubly dispersive channel as

$$\mathbf{r} = \mathbf{H}\mathbf{s} + \mathbf{w} = \sum_{p=1}^{P} h_p \mathbf{H}_p \mathbf{s} + \mathbf{w}, \tag{9}$$

where $h_p \in \mathbb{C}$ denotes the complex path gain of the p-th multipath component, identical to that of (1), (3), and (7), $\mathbf{H}_p$ is the circular convolutional matrix excluding the path gain coefficient h_p for the p-th path, $\mathbf{r} \in \mathbb{C}^{N\times 1}$ is the received signal vector collecting the N useful samples of $r[n]$ after discarding the prefix, and $\mathbf{w} \in \mathbb{C}^{N\times 1}$ represents the noise received per sample.

For the IDID and IDFD cases, where the normalized delays ℓ_p are integer-valued, the per-path channel matrix $\mathbf{H}_p$ can be decomposed as the product of a diagonal phase-rotation matrix and a cyclic permutation matrix, yielding [14], [20], [21], [41], [55]

$$\mathbf{H}_p = \mathbf{\Phi}_p \cdot \mathbf{V}^{f_p} \cdot \mathbf{\Pi}^{\ell_p} \in \mathbb{C}^{N\times N}. \tag{10}$$

The three matrix components in (10) are, respectively:

1) diagonal phase-offset matrix $\mathbf{\Phi}_p$, which models the phase-offset of the utilized prefix in (8) as

$$\begin{aligned}\mathbf{\Phi}_p &\triangleq \text{diag}(\boldsymbol{\phi}_p) \in \mathbb{C}^{N\times N} \\ &= \text{diag}\Big(\big[\underbrace{e^{-j2\pi\cdot\phi_{\text{cp}}(\ell_p)}, \cdots, e^{-j2\pi\cdot\phi_{\text{cp}}(1)}}_{\ell_p \text{ terms}}, \underbrace{1, \cdots, 1}_{N-\ell_p \text{ ones}}\big]\Big);\end{aligned} \tag{11}$$

2) diagonal Doppler shift matrix $\mathbf{V}^{f_p}$, which models the effect of the normalized digital Doppler shifts f_p based the N-th roots-of-unity matrix

$$\begin{aligned}\mathbf{V} &\triangleq \text{diag}(\mathbf{v}) \in \mathbb{C}^{N\times N} \\ &= \text{diag}\left(\left[1, e^{-j2\pi\frac{1}{N}}, \cdots, e^{-j2\pi\frac{N-1}{N}}\right]\right),\end{aligned} \tag{12}$$

which when raised to the f_p-th power as $\mathbf{V}^{f_p}$, is the diagonal matrix representing the phase rotation due to the Doppler shift; and

3) forward cyclic shift matrix $\mathbf{\Pi}^{\ell_p}$, which models the integer delay shift of ℓ_p samples, defined based on the single-step forward cyclic shift matrix $\mathbf{\Pi}$

$$\mathbf{\Pi} = \begin{bmatrix} 0 & 0 & \cdots & 0 & 1 \\ 1 & 0 & \cdots & 0 & 0 \\ 0 & 1 & \ddots & \vdots & \vdots \\ \vdots & \ddots & \ddots & 0 & 0 \\ 0 & \cdots & 0 & 1 & 0 \end{bmatrix} \in \mathbb{C}^{N\times N}, \tag{13}$$

such that left-multiplying a vector by $\mathbf{\Pi}$, *i.e.*, $\mathbf{\Pi}\mathbf{x}$, corresponds to a forward shift of $\mathbf{x}$, and therefore $\mathbf{\Pi}^{\ell_p}$ corresponds to a cyclic forward shift of ℓ_p indices.

As can be seen with the above formulation, the IDID and IDFD cases benefit from a highly sparse channel matrix $\mathbf{H}_p$, which consists of only a single non-zero element per row and column, due to the perfect alignment of the delays ℓ_p with the sampling grid (diagonal phase matrices and permutation matrix structure).

However, in the FDFD case with **non-integer** delays ℓ_p, it can be observed that such efficient formulations in (11) and (13) based on integer delays ℓ_p are no longer valid, in a similar construction to (7).

Namely, the separation of the phase-offset matrix and the shift matrix into independent diagonal and permutation operators $\mathbf{\Phi}_p$ and $\mathbf{\Pi}^{\ell_p}$ is no longer possible due to the inter-sample interference caused by fractional delays and the effective discrete-time pulse kernel $g(\cdot)$, and the generalized per-path FDFD channel matrix can be expressed as

$$\mathbf{H}_p \triangleq \mathbf{V}^{f_p} \cdot \mathbf{\Psi}(\ell_p) \in \mathbb{C}^{N\times N}, \tag{14}$$

where $\mathbf{V}^{f_p}$ models the sample-wise phase rotations due to the digital Doppler shift f_p, identical to the IDID and IDFD cases, while the new *chirp-periodically circulant* fractional delay matrix $\mathbf{\Psi}(\ell_p)$ captures the combined effect of the fractional delay and the corresponding prefix phase-offset, defined as

$$\mathbf{\Psi}(\ell_p) \triangleq \big(\mathbf{G}(\ell_p) + \mathbf{\Phi}(\ell_p)\big) \in \mathbb{C}^{N\times N}, \tag{15}$$

with the constituting effective interpolated delay matrix $\mathbf{G}(\ell_p)$ and the effective interpolated delay chirp-periodic prefix (CPP) matrix $\mathbf{\Phi}_p(\ell_p)$ defined element-wise as

$$[\mathbf{G}(\ell_p)]_{n,m} = g(n-m-\ell_p), \tag{16}$$

$$[\mathbf{\Phi}(\ell_p)]_{n,m} = g(n-m-\ell_p+N) \cdot e^{j2\pi\phi_{\text{cp}}(n-m-\ell_p)}, \tag{17}$$

where $\mathbf{G}(\ell_p)$ is generally dense and Toeplitz.

As illustrated in Fig. 1, for integer delays, the sum $\mathbf{G}(\ell_p) + \mathbf{\Phi}_p(\ell_p)$ perfectly reconstructs the sparse, phase-rotated cyclic permutation matrix used in legacy OFDM and AFDM literature, as evidenced by the identity between Fig. 1(a), based on (10), and Fig. 1(b), based on (14) and (15). Furthermore, the introduction of fractional delays in

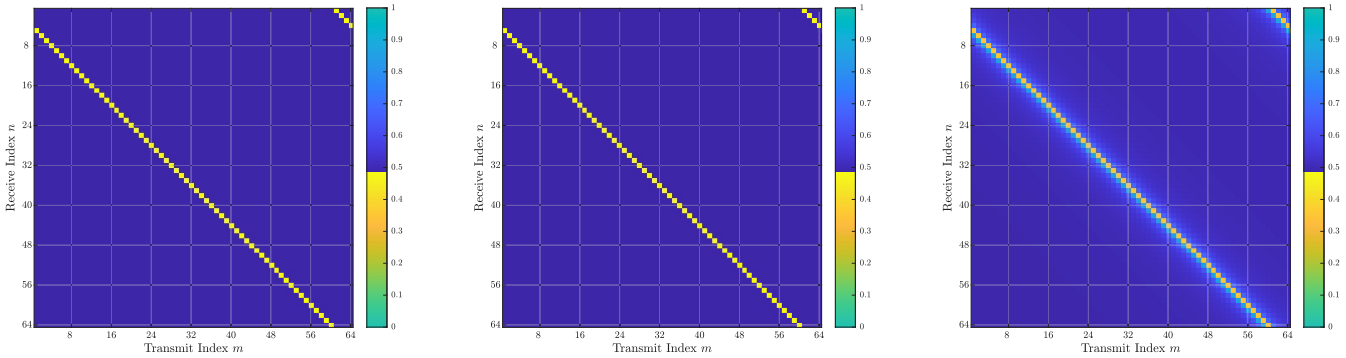

(a) Conventional IDID model following (10). (b) Generalized IDID model following (14). (c) Generalized FDFD model following (14).

FIGURE 1. Illustration of a single path within the channel matrix under IDID and FDFD scenarios, with $N = 64$. (a) shows the conventional IDID sparse permutation model of eq. (10) with $\ell_p = 4$ and $f_p = 2$; (b) shows the proposed generalized FDFD formulation of eq. (14) but under the same integer conditions; and (c) shows the proposed generalized FDFD formulation with fractional delay ($\ell_p = 4.3$) and fractional Doppler ($f_p = 2.1$), revealing the inter-sample coupling effects. The FDFD models in (b) and (c) are constructed based on the ideal band-limited pulse (Sinc interpolation).

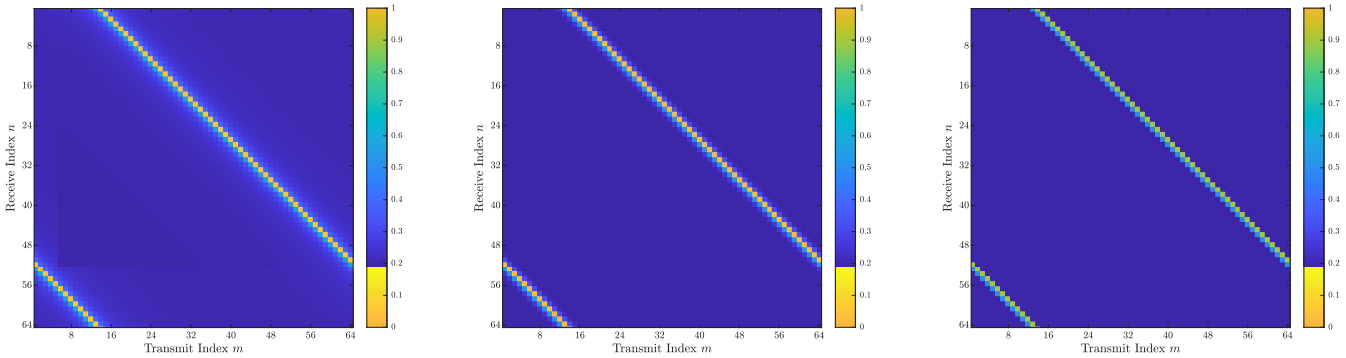

(a) Sinc (Ideal Band-limited) (b) Raised Cosine ($\alpha = 0.5$) (c) Rectangular (No Pulse Shaping)

FIGURE 2. Impact of different transmit pulse shapes $g(\cdot)$ on the single-path FDFD channel matrix $\mathbf{H}_p$ ($N = 64, \ell_p = 4.3, f_p = 2.1$), where the choice of the transmit filter governs the sparsity of the inter-sample coupling and the thickness of the diagonal band, while the main position of the shifted components remains unchanged and deterministic to the integer delay part $\lfloor \ell_p \rceil$.

Fig. 1(c) reveals the dense inter-sample coupling inherent to true 6G doubly dispersive channels,[1] where each received sample becomes a linear combination of all N transmitted samples.

This framework inherently therefore accommodates the transmit pulse-shape's influence on channel coupling, where the pulse-shape kernel $g(\cdot)$ affects inter-sample coupling. As illustrated in Fig. 2, under the ideal band-limited assumption (sinc interpolation kernel), the channel matrix exhibits the true inter-sample smearing and a consequently denser structure, distributing symbol energy across a wide band diagonal. In contrast, a rectangular pulse (non-pulse-shaped) yields a significantly sparser matrix with minimal inter-sample coupling, albeit with non-ideal spectral leakage and ICI. In between, a practical raised cosine pulse achieves better localization than the sinc kernel while capturing sufficient inter-sample coupling, and still obtains a sufficiently sparse structure exploitable for efficient estimation and detection algorithms.

[1]The proposed core FDFD channel model is readily extensible to broader doubly-dispersive channel scenarios [56], [57], [58].

Remark 1: To the best of our knowledge, the decomposition $\mathbf{\Psi}(\ell_p) = \mathbf{G}(\ell_p) + \mathbf{\Phi}(\ell_p)$ in (15)–(17) capturing the fractional delay effects with respect to the transmit pulse-shaping kernel in its explicit matrix form decoupled from the phase correction is a new contribution to the literature.

Although existing FDFD channel models are completely correct and identical numerically, the effects of fractional delays and the pulse-shaping filter components are absorbed into non-explicit element-wise descriptions of the channel elements. Consequently, these effects are not explicitly separated from the prefix-induced phase correction, and are often omitted in the analysis of AFDM and other waveforms proposed for doubly dispersive channels.

On the other hand, the proposed formulation explicitly incorporates the transmit pulse-shaping kernel $g(\cdot)$ as the Toeplitz matrix $\mathbf{G}(\ell_p)$, cleanly separating its contribution from the prefix-induced phase correction $\mathbf{\Phi}(\ell_p)$. This modular structure therefore unifies the IDID, IDFD, and FDFD cases under a single parametric framework (verified in Fig. 1(a)-(b)). It directly exposes the pulse-dependent sparsity of the effective channel matrix, which governs the complexity

and performance of the sparse detectors as will be further discussed in Section IV.

D. EXTENSION TO MIMO CHANNELS

The SISO FDFD model above extends naturally to MIMO channels with N_{t} transmit and N_{r} receive antennas via a standard Kronecker-product construction. For a uniform linear array (ULA) geometry, the per-path spatial signature is captured by the outer product $\mathbf{\Theta}_p = \mathbf{a}_{\mathrm{r}}(\theta_p^{\mathrm{r}})\mathbf{a}_{\mathrm{t}}^{\mathsf{H}}(\theta_p^{\mathrm{t}}) \in \mathbb{C}^{N_{\mathrm{r}}\times N_{\mathrm{t}}}$, where $\mathbf{a}_{\mathrm{t}}(\theta_p^{\mathrm{t}})$ and $\mathbf{a}_{\mathrm{r}}(\theta_p^{\mathrm{r}})$ denote the transmit and receive array response vectors, respectively. Stacking the N transmit sample vectors into $\bar{\mathbf{s}} \in \mathbb{C}^{N_{\mathrm{t}}N\times 1}$ and the received sample vectors into $\bar{\mathbf{r}} \in \mathbb{C}^{N_{\mathrm{r}}N\times 1}$, the blockwise MIMO FDFD model can be formulated as

$$\bar{\mathbf{r}} = \left(\sum_{p=1}^{P} h_p \cdot \mathbf{\Theta}_p \otimes \left(\mathbf{V}^{f_p} \cdot \mathbf{\Psi}(\ell_p)\right)\right) \cdot \bar{\mathbf{s}} + \bar{\mathbf{w}}, \tag{18}$$

where $\mathbf{\Psi}(\ell_p)$, $\mathbf{V}^{f_p}$ are as defined in (14). The channel structure exhibits the same per-block interference characteristics as in the SISO case, scaled by the per-path spatial signatures. Extensions to other array geometries (uniform planar arrays (UPAs), non-uniform arrays) and practical antenna correlation models [59] follow standard procedures and are omitted from the scope of this article.

III. ON THE COMPATIBILITY OF AFDM OVER OFDM

This section examines the AFDM modulator and demodulator structures in detail and shows that they require virtually no modifications to the underlying hardware architecture relative to legacy OFDM, particularly for the core transform processing, pulse shaping, resource allocation, and prefixing. All conventional OFDM modulator blocks can be reused directly, with only minimal additions in baseband processing. The OFDM and AFDM signal models are well-known background. The novel contribution of this section is the compatibility analysis in Section III-D built on top of them, establishing that OFDM and AFDM share the same underlying hardware and processing chain.

To that end, let us first introduce the input-output system model of the conventional OFDM and the AFDM modulator/demodulator, given the model of the discrete-time doubly dispersive channel.

A. OFDM SIGNAL MODEL

Let the k-th data symbol be denoted by $x_k \in \mathcal{X}$ for $k \in \{0,\dots,N-1\}$, where $\mathcal{X} \subset \mathbb{C}$ is the complex constellation set, with cardinality $|\mathcal{X}| = M$, *i.e.*, M-QAM or M-PSK.

Then, the OFDM transmit signal block with N samples in the time domain is generated via the inverse discrete Fourier transform (IDFT) as $\mathbf{s} = \mathbf{F}^{\mathsf{H}} \cdot \mathbf{x} \in \mathbb{C}^{N\times 1}$, where $\mathbf{s} \in \mathbb{C}^{N\times 1}$ is the transmit signal vector collecting one OFDM block in the time domain, $\mathbf{x} = [x_0,\dots,x_{N-1}]^T \in \mathbb{C}^{N\times 1}$ is the vector collecting the N data symbols, and $\mathbf{F} \in \mathbb{C}^{N\times N}$ is the N-point discrete Fourier transform (DFT) matrix.

For OFDM, the prefix required is a cyclic prefix (CP), and does not need a phase-offset per sample, and therefore, $\phi_{\mathrm{cp}}(\cdot) = 0$ and $\mathbf{\Psi}(\ell_p) = \mathbf{G}(\ell_p)$ in (15), yielding

$$\mathbf{r} = \left(\sum_{p=1}^{P} h_p \cdot \mathbf{V}^{f_p} \cdot \mathbf{G}(\ell_p)\right) \mathbf{F}^{\mathsf{H}} \cdot \mathbf{x} + \mathbf{w} \in \mathbb{C}^{N\times 1}. \tag{19}$$

On the receiver side, the OFDM demodulator applies the forward N-point normalized DFT to the received signal, yielding the frequency-domain received vector as

$$\mathbf{y} = \mathbf{F}\cdot\mathbf{r} = \underbrace{\mathbf{F}\left(\sum_{p=1}^{P} h_p \cdot \mathbf{V}^{f_p} \cdot \mathbf{G}(\ell_p)\right)\mathbf{F}^{\mathsf{H}}}_{\triangleq \mathbf{\Xi}^{\mathrm{OFDM}} \in \mathbb{C}^{N\times N}} \cdot \mathbf{x} + \mathbf{F}\mathbf{w} \in \mathbb{C}^{N\times 1}, \tag{20}$$

where, since the modulator and demodulator are independent of the path index p, the effective channel matrix describing the input-output relation of the data symbols can be expressed as the sum of the per-path effective channels, as

$$\mathbf{\Xi}^{\mathrm{OFDM}} \triangleq \sum_{p=1}^{P} h_p \cdot \mathbf{\Xi}_p^{\mathrm{OFDM}} \in \mathbb{C}^{N\times N}, \tag{21}$$

with $\mathbf{\Xi}_p^{\mathrm{OFDM}} \triangleq \mathbf{F}\cdot\mathbf{V}^{f_p}\cdot\mathbf{G}(\ell_p)\cdot\mathbf{F}^{\mathsf{H}} \in \mathbb{C}^{N\times N}$.

With integer delays and no Doppler shift, *i.e.*, $\mathbf{G}(\ell_p) = \mathbf{\Pi}^{\ell_p}$ and $\mathbf{V}^{f_p} = \mathbf{I}_N$, the effective channel matrix reduces to a completely diagonal matrix, which preserves the orthogonality among subcarriers and avoids inter-carrier interference: the defining characteristic of OFDM in static multipath channels.

However, when Doppler shifts are present, it is well known that the orthogonality among OFDM subcarriers is disrupted, leading to ICI. This effect is observed in the above model with the presence of $\mathbf{V}^{f_p} \neq \mathbf{I}_N$ introducing phase-rotations in the subcarriers, which no longer align with the Fourier basis. Therefore, off-diagonal elements appear in the effective channel matrix even when f_p is integer-valued, which are indistinguishable between paths.

For fractional Doppler or delay values, the effective channel becomes extremely dense, further increasing interference.

B. AFDM SIGNAL MODEL

To address the challenges posed by Doppler shifts identified above, the AFDM was proposed to convert the static subcarriers of OFDM into chirp-based subcarriers in the discrete affine Fourier transform (DAFT) basis.

The AFDM transmit block with N samples in the time domain is generated via the inverse discrete affine Fourier transform (IDAFT) as

$$\mathbf{s} = \mathbf{A}^{\mathsf{H}} \cdot \mathbf{x} \in \mathbb{C}^{N\times 1}, \tag{22}$$

where $\mathbf{A} \in \mathbb{C}^{N\times N}$ is the forward normalized DAFT matrix, which is unitary, described by

$$\mathbf{A} \triangleq \mathbf{\Lambda}_{\lambda_2}\mathbf{F}_N\mathbf{\Lambda}_{\lambda_1} \in \mathbb{C}^{N\times N}, \tag{23}$$

where $\mathbf{F}_N \in \mathbb{C}^{N\times N}$ is the N-point DFT matrix, and $\mathbf{\Lambda}_{\lambda_i} \triangleq \mathrm{diag}[e^{-j2\pi\lambda_i(0)^2},\cdots,e^{-j2\pi\lambda_i(N-1)^2}] \in \mathbb{C}^{N\times N}$ is a diagonal chirp

matrix defined by a central digital frequency λ_i, with two parametrizable chirp parameters λ_1 and λ_2.

Note that setting $\lambda_1 = \lambda_2 = 0$ yields the standard DFT, while $\lambda_1 = \lambda_2 = \frac{1}{2N}$ corresponds to the discrete Fresnel transform matrix utilized in orthogonal chirp division multiplexing (OCDM). Furthermore, the first chirp frequency λ_1 is a key parameter which can be optimized based on the channel statistics to ensure full diversity in doubly dispersive channels, namely by satisfying [20], [21]

$$\lambda_1 \geq \frac{2(f_{\max} + \xi) + 1}{2N}, \tag{24}$$

where $\lfloor f_{\max} \rceil \in \mathbb{Z}^+$ is the closest integer value of the maximum normalized Doppler shift $f_{\max}$, and $\xi \in \mathbb{Z}^+$ is a design parameter typically referred to as the *guard width* that provides a margin for robustness in Doppler.

On the other hand, the second chirp parameter λ_2 does not influence the orthogonality of AFDM over doubly dispersive channels. Instead, it serves as a flexible degree of freedom for tailoring time-domain waveform properties, such as the ambiguity function and PAPR characteristics.

To prevent spectral aliasing and ensure a unique signal representation, λ_2 is typically chosen such that $\lambda_2 \ll 1$ or $\lambda_2 \in \mathbb{R}\backslash\mathbb{Q}$ (*i.e.*, an irrational value), so that the phase progression of the second chirp does not periodically align with the discrete sampling grid. The necessary prefix in AFDM is a CPP to ensure circular convolution under chirp-domain periodicity, determined by the phase-offset function $\phi_{\text{cp}}^{\text{AFDM}}(n) = \lambda_1(N^2 + 2Nn)$, making $\mathbf{\Phi}_p$ in (11) non-identity.

However, it is also known that for specific configurations of the AFDM parameters, namely when $2N\lambda_1$ is an even integer, the CPP reduces to a conventional CP without phase offsets, *i.e.*, $\phi_{\text{cp}}^{\text{AFDM}}(n) = 0$ for all n, and therefore $\mathbf{\Phi}_p = \mathbf{I}_N$.

The received signal after passing through the doubly dispersive channel in the general FDFD case is then expressed as

$$\mathbf{r} = \left(\sum_{p=1}^{P} h_p \cdot \mathbf{\Phi}_p \cdot \mathbf{V}^{f_p} \cdot \mathbf{G}(\ell_p) \right) \mathbf{A}^{\mathsf{H}} \cdot \mathbf{x} + \mathbf{w} \in \mathbb{C}^{N \times 1}. \tag{25}$$

At the receiver, the demodulator applies the matched forward DAFT, *i.e.*, with the same parametrization of λ_1 and λ_2, yielding the received vector $\mathbf{y} = \mathbf{A} \cdot \mathbf{r}$ in the affine-frequency domain as

$$\mathbf{y} = \mathbf{A} \left(\sum_{p=1}^{P} h_p \cdot \mathbf{\Phi}_p \cdot \mathbf{V}^{f_p} \cdot \mathbf{G}(\ell_p) \right) \mathbf{A}^{\mathsf{H}} \cdot \mathbf{x} + \mathbf{A}\mathbf{w} \tag{26}$$

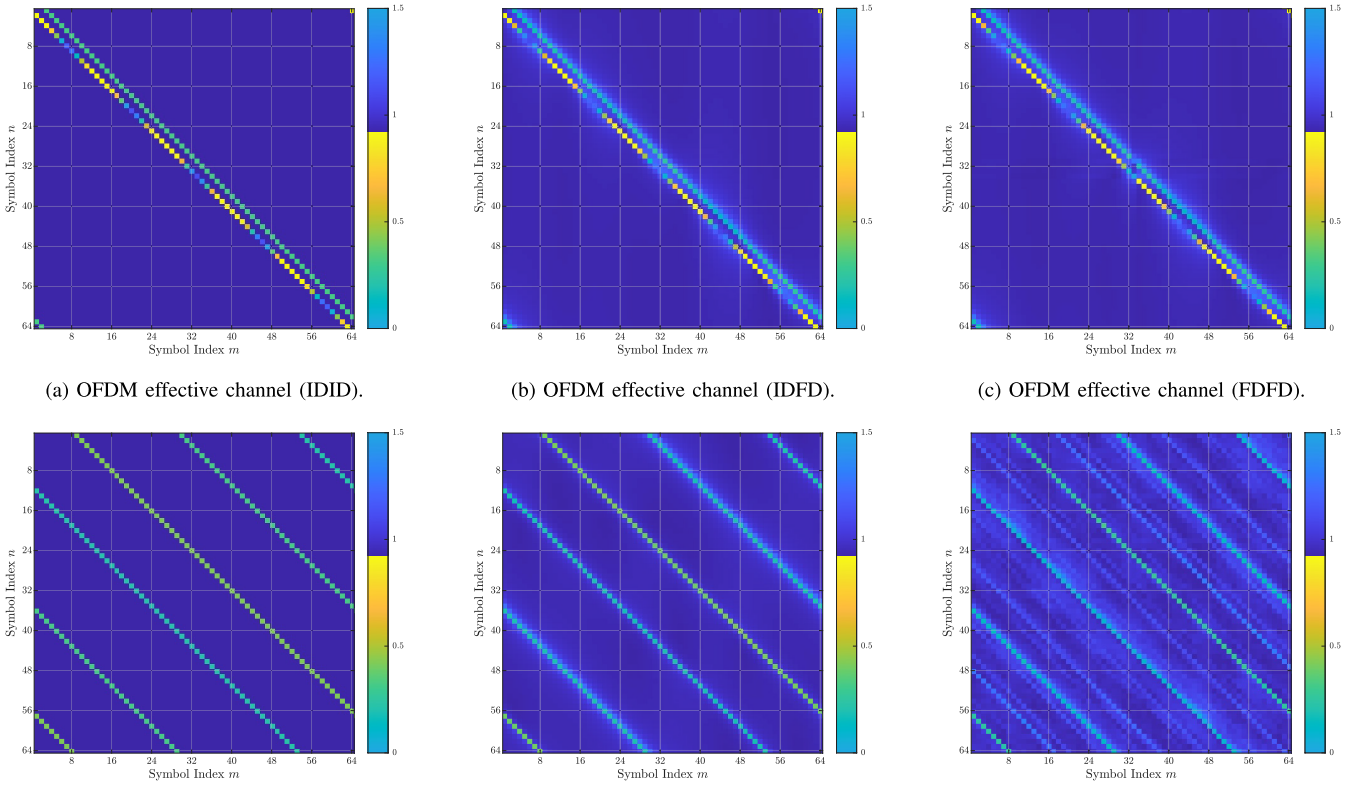

(a) OFDM effective channel (IDID). (b) OFDM effective channel (IDFD). (c) OFDM effective channel (FDFD).

(d) AFDM effective channel (IDID). (e) AFDM effective channel (IDFD). (f) AFDM effective channel (FDFD).

FIGURE 3. **Effective channel matrices Ξ for OFDM and AFDM, respectively on the first and second rows, in a 3-path doubly dispersive scenario with $N = 64$. The physical channel parameters are defined by path coefficients $\{1, 0.9, 0.8\}$, normalized delays $\{1.3, 3.25, 5.96\}$, and normalized digital Dopplers $\{1.1, -2.3, 0.85\}$, where for the IDID and IDFD cases, the delays and Dopplers are rounded to the nearest integers as relevant. For the AFDM implementation, chirp parameters are set to $c_1 = (2(f_{\max} + 1) + 1)/2N$, with $f_{\max} = 3$, and $c_2 = 1/2N$. It can be seen that on top of the discussed effects of the fraction taps in Section II-C, the different paths of the OFDM effective channel matrices are indistinguishable under Doppler shifts, leading to significant inter-carrier interference, while AFDM maintains a more distinguishable effective channel matrix, preserving better orthogonality.**

with $\boldsymbol{\Xi}^{\text{AFDM}} \triangleq \sum_{p=1}^{P} h_p \cdot \boldsymbol{\Xi}_p^{\text{AFDM}}$, where $\boldsymbol{\Xi}^{\text{AFDM}}$ represents the structural effective channel matrix describing the input-output relation of the data symbols between the AFDM modulator and demodulator, which, as in the OFDM case, can be expressed as the sum of the per-path components and the channel fading coefficients, with $\boldsymbol{\Xi}_p^{\text{AFDM}} \triangleq \mathbf{A}\boldsymbol{\Phi}_p\mathbf{V}^{f_p}\mathbf{G}(\ell_p)\mathbf{A}^{\mathsf{H}} \in \mathbb{C}^{N\times N}$.

The OFDM and AFDM effective channels have been illustrated for the IDID, IDFD, and FDFD cases in Fig. 3.

C. MIMO EXTENSION OF OFDM AND AFDM SIGNAL MODELS

The MIMO signal model of OFDM and AFDM follows from a block-wise application of the modulator and demodulator to a stacked model, replacing the SISO channel part in (18) with the effective channel including the modulator operations, i.e.,

$$\bar{\mathbf{y}}^{\text{MIMO-OFDM}} = \left(\sum_{p=1}^{P} h_p \cdot \boldsymbol{\Theta}_p \otimes \boldsymbol{\Xi}_p^{\text{OFDM}}\right)\bar{\mathbf{x}} + \tilde{\mathbf{w}}, \tag{27}$$

$$\bar{\mathbf{y}}^{\text{MIMO-AFDM}} = \left(\sum_{p=1}^{P} h_p \cdot \boldsymbol{\Theta}_p \otimes \boldsymbol{\Xi}_p^{\text{AFDM}}\right)\bar{\mathbf{x}} + \tilde{\mathbf{w}}. \tag{28}$$

Trivially, the channel structure exhibits the same per-block interference characteristics as in the SISO case, but with the corresponding antenna response coefficients across antennas.

D. A NOTE ON OFDM AND AFDM COMPATIBILITY

For the modulator/demodulator, the fundamental DAFT/IDAFT steps require only a core FFT/IFFT block and two subcarrier-wise (element-wise) phase-rotation blocks, as described in (23). Thus, for any parametrization of the AFDM, these two phase-rotation blocks (highlighted in blue) are placed immediately before and after the FFT/IFFT block (highlighted in green), as illustrated in Fig. 4.

This phase-rotation mechanism is already widely adopted in conventional OFDM systems and techniques, such as: *Selected Mapping (SLM)* method for PAPR reduction, where each OFDM symbol is multiplied by a unit-magnitude phase vector before the IFFT [60], *Cyclic Delay Diversity (CDD)* technique adopted in LTE, where transmit antennas apply linearly varying per-subcarrier phase rotations to achieve frequency diversity [61], *pilot phase randomization* in IEEE 802.11 WLANs, where predefined phase sequences modulate pilot subcarriers to aid carrier tracking [62], and *pilot scrambling* in DBV-T, where pilot tones are multiplied by a pseudo-random binary phase to reduce interference [63].

Furthermore, the remaining baseband processing blocks, such as resource mapping for pilots and subcarrier allocation, can be directly reused, since the resources in AFDM are indexed in a one-dimensional (affine) frequency domain. Similarly, the prefix is prepended along this single dimension, followed by a time-domain windowing block applied identically to that of conventional OFDM. In summary, AFDM does not require any changes to the physical transceiver hardware, introducing only lightweight baseband chirp rotations and CPP phase adjustments.

This high level of structural compatibility between AFDM and OFDM contrasts with OTFS, which requires several structural modifications beyond standard OFDM for a mathematically compliant implementation. The OTFS waveform is inherently defined in the delay-Doppler domain and relies on either an inverse symplectic finite Fourier transform (ISFFT) combined with the Heisenberg transform (HT), or the inverse discrete Zak transform (IDZT), to transform the delay-Doppler symbols into a time-domain sequence [42]. When assuming the non-ideal rectangular pulses for interpolation and upsampling, this combination of ISFFT and HT collapses into the IDZT, which can be efficiently implemented using interleavers and multiple lower-dimensional IDFTs. However, in practical doubly dispersive channels with non-integer Dopplers and delays, the necessary bi-orthogonality property of the OTFS basis is not fully satisfied under such non-ideal rectangular pulses, and therefore complex pulse-shaping is necessary as will be further elaborated in the following.

E. PULSE-SHAPING, WINDOWING, AND PREFIXING BLOCKS

Pulse-shaping is an important criterion in the discrete-time modeling and practical realization of multicarrier waveforms in doubly dispersive channels. The legacy OFDM systems (e.g., LTE, 5G NR, Wi-Fi) traditionally employ an implicit rectangular pulse (i.e., no pulse-shaping) along-side a cyclic prefix, which still ensures orthogonality in static multipath channels. In a general case, however, additional spectral containment may be desired, especially under high-mobility channels, implemented by a time-domain windowing framework (sometimes simply called OFDM pulse-shaping), where a real-valued filter is applied sample-wise prior to the digital-to-analog conversion (DAC), i.e.,

$$\mathbf{s}_{\text{ps}} = \text{diag}(\mathbf{p}) \cdot \mathbf{s}_{\text{cp}} = \mathbf{p} \odot \mathbf{s}_{\text{cp}} \in \mathbb{C}^{(N+N_{\text{cp}})\times 1}, \tag{29}$$

where $\mathbf{s}_{\text{cp}} \in \mathbb{C}^{(N+N_{\text{cp}})\times 1}$ is the modulator output vector including a cyclic prefix of length N_{cp}, and $\mathbf{p} \in \mathbb{R}^{(N+N_{\text{cp}})\times 1}$ is the real-valued windowing filter, and $\mathbf{s}_{\text{ps}} \in \mathbb{C}^{(N+N_{\text{cp}})\times 1}$ is the windowed transmit signal vector.

For the AFDM, the modulator and demodulator architecture admit the same generic pulse-shaping operation without altering hardware, employing the same digital filter in (29) as OFDM prior to transmission, as the subcarrier orthogonality in time-frequency domain is guaranteed by the underlying unitary basis function DAFT and the CPP ensures circular convolutional structure under chirp-periodicity, just as the OFDM's DFT basis with CP, although some non-ideal spectral properties may arise [64].

However, as mentioned before, the more critical case is OTFS, whose theoretically ideal bi-orthogonality in delay-Doppler cannot be fully satisfied in practical systems with finite signal support, especially under rectangular pulses. In such cases, the practical OTFS input-output relation departs from the theoretical delay-Doppler convolution model, suffering a loss of bi-orthogonality that necessitates complex equalization. Therefore, OTFS generally requires dedicated

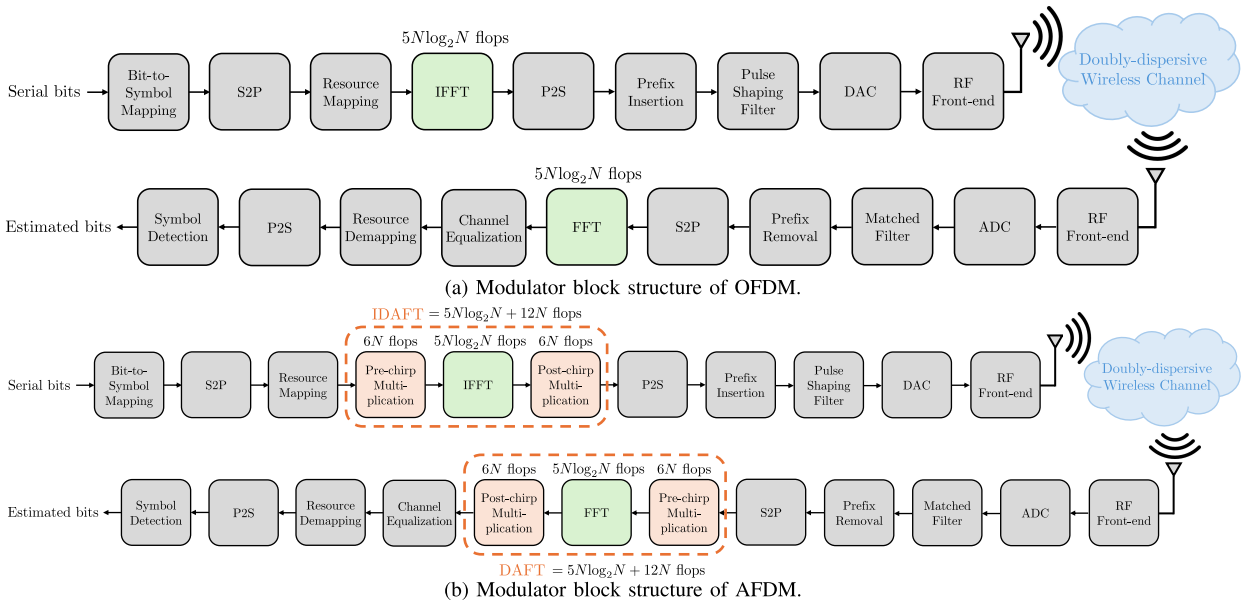

FIGURE 4. Comparison of OFDM and AFDM transceiver structures, which highlights that the only structural difference lies in the two element-wise chirp-phase rotations (pre- and post-multiplications) surrounding the IFFT/FFT blocks from the conventional OFDM transceivers.

pulse-shaping in the interpolating upsampler to mitigate the loss of bi-orthogonality (which is approached but not exactly achieved under finite support), a limitation not present in OFDM and AFDM whose channel and modulation basis remain mutually orthogonal for arbitrary pulse shapes.

One approach of pulse shaping for OTFS is to apply a time-domain pulse-shaping HT after the ISFFT, which can mitigate some non-idealities but remains fundamentally limited by finite support and the Balian-Low constraints. However, the non-rectangular pulse-shaping HT implies that the OTFS modulator requires three consecutive FFT/IFFT operations with interleaving and reshaping, which cannot be reduced further as commonly assumed for the rectangular pulse case, leading to increase in complexity and latency.

Alternatively, recent work on Zak-OTFS introduces a direct delay-Doppler domain pulse-shaping approach, which eliminates the need for the ISFFT and HT, but instead requires a two-dimensional convolution in the delay-Doppler domain for the pulse shaping before the single IDZT. This DD-domain filtering enables more controlled localization and yields the closest practical approximation to the ideal twisted convolution, although perfect bi-orthogonality remains unattainable under finite time-bandwidth constraints.

Thus, careful pulse shaping is necessary for OTFS to retain its desired structural characteristics in practical doubly-dispersive channels, whereas AFDM and OFDM preserve their orthogonality and convolutional forms even with simple rectangular pulses.

Furthermore, unlike AFDM, where a one-dimensional cyclic prefix (with chirp periodicity) is sufficient to ensure robustness, OTFS has recently been shown to require a so-called double cyclic prefix (in both time and frequency dimensions) to improve its robustness on top of the single time-domain cyclic prefix [65]. This unique prefixing strategy necessitates a distinct resource allocation and indexing scheme, and also leads to increased signaling overhead and complexity.

Overall, this section shows that AFDM preserves the core OFDM hardware pipeline and one-dimensional framing structure, requiring only lightweight digital chirp rotations and a re-parameterized cyclic prefix, without introducing new baseband modules or RF redesign. In contrast, OTFS operates in a distinct modulation domain and, under practical pulse-shaping conditions for doubly dispersive channels, requires 2D processing and non-native prefixing and resource grids,

TABLE 1. Computational Complexity of Key Operations and Total Modulator/Demodulator Complexities in FLOP, with $N = KL$.

Operation	Complexity (FLOPs)
IDFT_N	$5N\log_2 N$
IDAFT_N	$5N\log_2 N$
$\mathrm{ISFFT}_{K,L}$	$5N\log_2 N$
$\mathrm{HT}_{K,L}$	$5N\log_2 L + 2N$
$\mathrm{IDZT}_{K,L}$	$5N\log_2 L$
1D pulse shaping	$12N$
DD pulse shaping	$10N\log_2 N + 6N$

Pulse-shaped Waveform	Complexity (FLOPs)
OFDM	$5N\log_2 N$
AFDM	$5N\log_2 N + 12N$
OTFS	$5N\log_2 N + 5N\log_2 L + 2N$
Zak-OTFS	$10N\log_2 N + 5N\log_2 L + 6N$

leading to higher integration complexity relative to OFDM (see Table 1). While simplified rectangular-pulse OTFS implementations can partially reuse OFDM hardware, full bi-orthogonal implementations incur the multi-stage overhead quantified above. Consequently, AFDM is shown to be a hardware- and specification-efficient evolutionary waveform candidate for next-generation systems.

IV. ANALYSIS OF THE AFDM TRANSCEIVER OVER OFDM

Each subsection surveys existing AFDM algorithms and techniques to provide a unified picture of the transceiver. The distinguishing contribution of this section is the systematic analysis of each layer's compatibility with the OFDM legacy, and its behavior under the generalized FDFD channel model of Section II. Where specific results are drawn from prior works, they are cited accordingly. The FDFD-contextualized analyses, the layer-by-layer comparison against OFDM counterparts, and the structural observations on sparsity and reusability are new contributions of this article.

A. MODULATION COMPLEXITY AND SCALABILITY

Drawing from the previous section, the additional computational burden of the AFDM modulator/demodulator relative to conventional OFDM stems only from the two chirp-domain element-wise phase rotations applied immediately before and after the FFT/IFFT stage; all other blocks are identical and can be reused directly (excluding channel equalization), as shown in Fig. 4. Thereby, each complex phase rotation over N samples (equivalent to the number of subcarriers) is implemented simply via N element-wise complex multiplications, which require a total of $6N$ floating point operations (FLOPs). Hence, the two rotations introduce an extra cost of $12N$ FLOPs per AFDM symbol block of N complex symbols.

With the conventional Q-point FFT/IFFT cost given by $C_{\text{FFT},Q} \triangleq 5Q\log_2 Q$ FLOPs, the total per-block modulator/demodulator complexity for AFDM with N symbols is then obtained as

$$C_{\text{AFDM},N} = 5N\log_2 N + 12N \quad \text{[FLOPs]}. \tag{30}$$

By comparison, the conventional OFDM modulator cost is trivially given by the complexity of the N-point IFFT/FFT blocks directly, i.e., $C_{\text{OFDM},N} = C_{\text{FFT},N}$. Therefore, the relative complexity overhead of AFDM over OFDM is

$$\frac{C_{\text{AFDM},N} - C_{\text{OFDM},N}}{C_{\text{OFDM},N}} = \frac{12N}{5N\log_2 N} = \frac{12}{5\log_2 N}. \tag{31}$$

For practical FFT/IFFT sizes (number of subcarriers) considered in 6G, the overhead in (31) evaluates to modest values, with $N = 256$ amounting to a 30% overhead, $N = 1024$ to 24%, and $N = 4096$ to 20%. Hence, although the chirp rotations are neither cost-free nor negligible, their asymptotic impact diminishes logarithmically as the number of subcarriers grows, and the FFT/IFFT remains the dominant complexity term.

Next, as a reference and comparison, we provide a similar analysis for the OTFS. For the ISFFT + HT approach with the OTFS delay-Doppler frame of size $K \times L$, where we set $N = KL$ to fairly compare the different waveforms in terms of the resource usage (i.e., number of discrete symbol resources), the total complexity of the ISFFT, which is implemented using L IFFTs of size K, and K FFTs of size L, is given by

$$\begin{aligned} C_{\text{ISFFT},KL} &= L(5K\log_2 K) + K(5L\log_2 L) \ \text{[FLOPs]} \\ &= 5KL(\log_2 KL) = 5N\log_2 N = C_{\text{FFT},N}, \end{aligned} \tag{32}$$

i.e., the same as a single N-point IFFT for $N = KL$.

Then, a pulse-shaped HT is performed, consisting of K successive IFFT operations of length L, each followed by a complex-real time-domain scaling that applies the prototype pulse, with an additional computational complexity of

$$\begin{aligned} C_{\text{HT},KL} &= K(5L\log_2 L) + 2KL \quad \text{[FLOPs]} \\ &= N(5\log_2 L + 2). \end{aligned} \tag{33}$$

In all, the total complexity of the ISFFT-HT based OTFS modulator/demodulator is then given by

$$\begin{aligned} C_{\text{OTFS},KL} &= C_{\text{ISFFT},KL} + C_{\text{HT},KL} \\ &= 5N(\log_2 NL) + 2N. \ \text{[FLOPs]} \end{aligned} \tag{34}$$

Alternatively, if pulse-shaping is performed directly in the delay-Doppler domain via 2D convolution in the prior, a single IDZT approach may be employed. The IDZT on a $K \times L$ delay-Doppler block is implemented using K IFFTs of length L with some sample interleaving operation, where the latter is approximated to have negligible computation complexity (only space complexity), such that the total complexity required for the IDZT is

$$C_{\text{Zak}} = K\big(5L\log_2 L\big) = 5N\log_2 L. \ \text{[FLOPs]} \tag{35}$$

The 2D convolution for the pulse shaping in the delay-Doppler grid of size $K \times L$, is efficiently implemented using an FFT-based approach instead of the inefficient naive convolution, which involves a forward 2D FFT, a point-wise multiplication with the pulse's 2D FFT, and an inverse 2D FFT back to the delay-Doppler, i.e.,

$$\mathbf{X}_{\text{DD,ps}} = \text{IDFT}_{\text{2D}}\Big(\text{DFT}_{\text{2D}}(\mathbf{X}_{\text{DD}}) \odot \text{DFT}_{\text{2D}}(\mathbf{P})\Big), \tag{36}$$

where $\mathbf{X}_{\text{DD}} \in \mathbb{C}^{K\times L}$ is the delay-Doppler symbol block, $\mathbf{P} \in \mathbb{R}^{K\times L}$ is the real-valued pulse shaping filter in the delay-Doppler domain, and $\mathbf{X}_{\text{DD,ps}} \in \mathbb{C}^{K\times L}$ is the pulse-shaped delay-Doppler symbol block.

We may assume that the complexity of obtaining the FFT of the pulse filter, $\text{DFT}_{\text{2D}}(\mathbf{P})$, is negligble as it can be computed offline once, therefore the computational complexity is obtained for one FFT of size $K \times L$, one IFFT of size $K \times L$, and the element-wise multiplication of two matrices of size $K \times L$, yielding a total complexity of

$$\begin{aligned} C_{\text{DDps},KL} &= 2 \cdot (5KL\log_2 KL) + 6KL \quad \text{[FLOPs]} \\ &= 10N\log_2 N + 6N. \end{aligned} \tag{37}$$

Therefore, in all, the total complexity of the Zak-OTFS modulator/demodulator with delay-Doppler pulse shaping is approximated as

$$\begin{aligned} C_{\text{Zak-OTFS}} &= C_{\text{Zak}} + C_{\text{DDps},KL} \quad [\text{FLOPs}] \\ &= 5N\log_2 L + 10N\log_2 N + 6N \\ &= 5N\log_2(LN^2) + 6N \end{aligned} \tag{38}$$

Comparing the modulator complexities including the pulse-shaping overheads of OFDM, AFDM, and the two OTFS implementations in (34) and (38), which are summarized in Table 1, it is evident that both OTFS approaches introduce significantly higher computational burdens compared to the OFDM due to their multi-stage transform structures and 2D processing requirements under practical systems,[2] while AFDM maintains a modest overhead over OFDM and therefore represents a more computationally efficient alternative.

In addition to arithmetic complexity, memory movement and on-chip buffering often dominate latency and energy consumption in practical modems, especially in high-throughput systems. In this perspective, the AFDM waveform requires only local element-wise multiplications for its additional processing, which do not necessitate global data reshaping beyond the existing FFT/IFFT buffering inherent in the system. Conversely, OTFS implementations may involve more complex data handling due to frequent reshaping operations under practical, non-ideal conditions, such as interleaving and reshaping required in the ISFFT and pulse shaping stages.

Beyond per-block complexity, we consider how AFDM and OTFS scale with the number of subcarriers and antennas, especially for practical MIMO systems at high bandwidths and data rates. Since the computational complexity and memory requirements of both AFDM and OTFS scale linearly with the antenna count in MIMO systems, the relative overheads identified above remain consistent regardless of that count, so the previous analysis applies directly to massive MIMO deployments for 6G+.

B. PILOT SCHEME AND CHANNEL ESTIMATION

In this section, we discuss channel estimation strategies for AFDM in doubly dispersive channels, focusing on pilot design and estimation algorithms. Given the structural similarities between AFDM and OFDM, many established pilot schemes can be adapted to AFDM, albeit with modifications to account for the unique characteristics of the affine-frequency domain.

1) PILOT SCHEMES

Due to the structure of the effective channel matrix Ξ^{AFDM} as described in Section III-B, the usual pilot schemes for AFDM involve one or multiple pilot subcarriers [21], [66], each of which is isolated from other subcarriers by guard bands (in the DAFT domain) to capture the contribution of each path without interference properly.

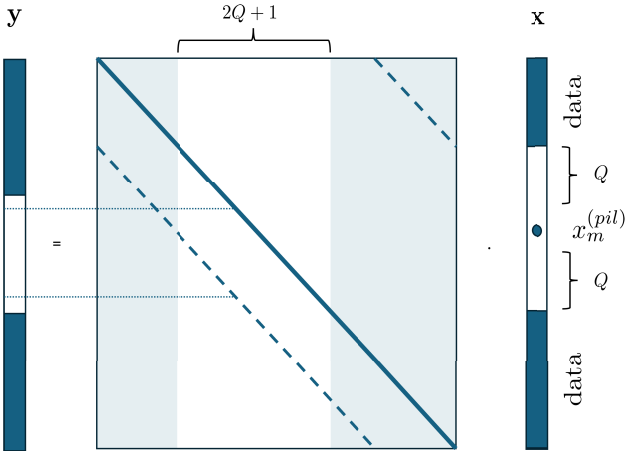

FIGURE 5. Transmitted pilot vector multiplexed with data x (as in 39) in the affine-frequency domain and received signal y.

In the case of the conventional single-pilot scheme [21], the transmitted symbol vector $\mathbf{x} \in \mathbb{C}^{N\times 1}$ in the affine-frequency domain is designed as

$$\begin{aligned} \mathbf{x} = [&x_0, \ldots, x_{m-Q}, \\ &\underbrace{0, \ldots, 0}_{Q}, x_m^{(\text{pil})}, \underbrace{0, \ldots, 0}_{Q}, x_{m+Q}, \ldots, x_{N-1}]^{\mathsf{T}}, \end{aligned} \tag{39}$$

where $x_m^{(\text{pil})}$ is the pilot at position m in the vector, surrounded by Q null subcarriers that serve as a guard band, and the remaining subcarriers are used to transmit data symbols, as shown in Fig. 5.

Note that to avoid interference from the data subcarriers, the guard band width Q must satisfy [21], [66]

$$Q \geq (\ell_{max} + 1)(2f_{\max} + 1) - 1, \tag{40}$$

where ℓ_{max} and $f_{\max}$ are the maximum normalized delay and maximum normalized digital Doppler shift of the doubly dispersive channel, respectively.

In the case of a multiple-pilot aided scheme, the pilot subcarriers must be separated by a distance of at least Q, which can improve the channel estimation performance (through the diversity of pilots), at the expense of a loss of spectral efficiency (SE), since each additional pilot involves at least $Q+1$ subcarriers not used for data transmission.

To circumvent the SE loss, a guard interval-free pilot scheme has been proposed in [67], where the $2Q$ null subcarriers in (39) are substituted by data. Alternatively, a superimposed pilot scheme is also described in [68], theoretically optimizing the SE. In this case, pilot subcarriers $x_m^{(\text{pil})}$ are superimposed to the data x_m (*i.e.* $x_m + x_m^{(\text{pil})}$), with a distance Q between the added pilots. However, in both

[2]Regarding FFT dimension flexibility, OFDM and AFDM support arbitrary FFT/IFFT sizes N with one-dimensional frequency-domain processing, enabling flexible numerology and resource allocation. In contrast, OTFS imposes strict integer divisibility constraints on the delay-Doppler grid dimensions $K, L \in \mathbb{N}$ such that $N = KL$, limiting design flexibility and potentially resulting in awkward FFT sizes for practical implementations and efficient computations.

cases, channel estimation and data detection require specific processing at the receiver side, as discussed in the following.

For a negligible Doppler shift, or when all paths share a common Doppler shift and integer delays (a usual assumption in OFDM systems), the channel frequency response and the Doppler shift can be estimated separately in the frequency and time domains, respectively [69], while estimation in the DAFT domain remains practicable. To this end, a single pilot aided scheme as in (39) can be considered without data multiplexing, i.e. $\mathbf{x}$ consists of $N-1$ null subcarriers with only one pilot $x_m^{(\text{pil})}$ at the m-th position.

In the frequency domain, the pilot vector is given by $\mathbf{x}_f = \mathbf{F}\cdot\mathbf{A}^{\mathsf{H}}\cdot\mathbf{x}$, which is not tractable in general. However, according to [69] and [70], $\mathbf{x}_f$ has a simple and tractable expression in the special case of $q = 2N\lambda_1 \in \mathbb{Z}$, where the non-zero elements of $\mathbf{x}_f$ are then constant modulus and equi-spaced with a distance $|q|$ between two consecutive pilot subcarriers in the frequency domain, starting with subcarrier $m_q = (m)_{|q|}$. Interestingly, setting $|q| \in \{2, 4\}$, the pilot scheme is very similar to the pilot distribution described for the 5G signals [71], so that the estimation processing used for 5G signals can be used in AFDM. Furthermore, to limit the SE loss, it is also possible to multiplex pilot and data in the frequency domain or in the DAFT domain as in (39).

2) CHANNEL ESTIMATION IN THE DAFT DOMAIN

In this section, we present the basics of channel estimation in the DAFT domain based on the pilot scheme described in (39). Other methods will be briefly discussed afterwards.

a: INTEGER DELAY AND DOPPLER

The estimation of the channel necessitates the estimation of $3P$ unknown parameters corresponding to the delay ℓ_p, the Doppler shift f_p, and the complex gain h_p for each of the paths $p = \{1, \ldots, P\}$. As raised by the authors in [21], the common maximum likelihood (ML) estimation of the $3P$ parameters is intractable in practice. However, it is possible to estimate the parameters separately, as described below. First, it must be noticed that by substituting (39) into (26), we find that the elements y_k of $\mathbf{y}$, for $k \in \left\{\left(m-(Q-f_{\max})\right)_N, \left(m+f_{\max}\right)_N\right\}$ are given by [45]

$$y_k = \begin{cases} [\mathbf{\Xi}^{\text{AFDM}}]_{k,m}\cdot x_m^{(\text{pil})} + [\mathbf{Aw}]_k \\ \qquad \text{if } k = \left(m+N-\text{loc}_p\right)_N, \\ [\mathbf{Aw}]_k \qquad \text{otherwise,} \end{cases} \tag{41}$$

where $\text{loc}_p = \left(f_p + \ell_p(2f_{\max}+1)\right)_N$.

This is illustrated in Fig. 5. Then, for any $\ell = \{0, 1, \ldots, \ell_{\max}\}$, the ML estimation of f_ℓ is given by

$$\hat{f}_\ell = \underset{k'\in\Omega_{k'}}{\arg\max}\ |y_k|^2, \tag{42}$$

where $\Omega_{k'} = [-f_{\max}, f_{\max}]$ and $k = \left(l\cdot 2f_{\max}+k'\right)_N$.

If the number of paths P is known *a priori*, it corresponds to the P highest values of $|y_k|^2$ among the $\ell_{\max}$ calculated in (42). If P is unknown, it is suggested in [66] to set a threshold ζ depending on the SNR and to keep the P paths whose value $|y_k|^2$ exceeds ζ.

Once (f_p, ℓ_p), for $p = \{1, \ldots, P\}$ is estimated, the estimate of the complex gains h_p can be obtained through

$$\hat{h}_p = \frac{\left[\mathbf{\Xi}^{\text{AFDM}'}\right]^*_{k_p,m}\cdot y_{k_p}}{x_m^{(\text{pil})}} \tag{43}$$

where $k_p = \left(\ell_p\cdot 2f_{\max}+f_p\right)_N$, and the value $[\mathbf{\Xi}^{\text{AFDM}'}]_{k_p,m}$ is generated using the estimates $(\hat{f}_p, \hat{\ell}_p)$.

b: INTEGER DELAY AND FRACTIONAL DOPPLER

In this part, we denote the integer and fractional parts of f_p by $f_p^{(i)} = \lfloor f_p \rceil$ and $f_p^{(f)} = f_p - f_p^{(i)}$, respectively. As introduced in [21], the estimation of the $3P$ channel parameters in the case of fractional Doppler starts by the estimation of the integer part $f_p^{(i)}$ as in (41)-(42). Then, the fractional part $f_p^{(f)}$ is estimated through

$$\hat{f}_p^{(f)} = \underset{f_p^{(f)}\in\left[-\frac{1}{2},\frac{1}{2}\right]}{\arg\max}\ \frac{\sum_{k'\in\Omega_{k'}}\left|\left[\mathbf{\Xi}^{\text{AFDM}'}\right]^*_{k,m}y_k\right|^2}{\sum_{k'\in\Omega_{k'}}\left|\left[\mathbf{\Xi}^{\text{AFDM}'}\right]_{k,m}\right|^2}, \tag{44}$$

where $k = \left(\ell_p\cdot 2f_{\max}+k'\right)_N$, and the value $[\mathbf{\Xi}^{\text{AFDM}'}]_{k_p,m}$ is generated using the estimates $(\hat{f}_p = \hat{f}_p^{(i)} + f_p^{(f)}, \hat{\ell}_p)$.

Moreover, in practice, (44) is performed using a search on a fine discretization of $\left[-\frac{1}{2}, \frac{1}{2}\right]$, such that ultimately, the estimate of the complex gains h_p can be obtained through

$$\hat{h}_p = \frac{\sum_{k'\in\Omega_{k'}}\left[\mathbf{\Xi}^{\text{AFDM}'}\right]^*_{k,m}y_k}{x_m^{(\text{pil})}}, \tag{45}$$

where the value $[\mathbf{\Xi}^{\text{AFDM}'}]_{k_p,m}$ is generated using the estimates $(\hat{f}_p = \hat{f}_p^{(i)} + \hat{f}_p^{(f)}, \hat{\ell}_p)$.

c: FRACTIONAL DELAY AND DOPPLER

Finally, the problem of estimating both fractional delay and Doppler parameters can be particularly difficult or even untractable if $\mathbf{G}(\ell_p)$ is dense and Toeplitz as suggested in (16). However, according to the finite interpolation kernel, $\mathbf{G}(\ell_p)$ (and as illustrated in Figure 2) is a banded matrix with a relatively tight band diagonal of defined width $2B+1$.

Furthermore, the matrix $\mathbf{G}(\ell_p)$ can be approximated to be circulant instead of Toeplitz, which becomes exact if a cyclic suffix is also used in addition to the CPP, or if a negative delay is applied previous to the demodulation process. In light of the above, by denoting $[g_{-B}, .., g_0, .., g_B]$ as the non-zero coefficients of the band diagonal of $\mathbf{G}(\ell_p)$, where $g_q = g(q-\ell_p)$, $p = -B, .., B$, $\mathbf{G}(\ell_p)$ can be rewritten as

$$\mathbf{G}(\ell_p) = \sum_{q=-B}^{B} g_q\cdot\mathbf{\Pi}^{\ell_p+q}. \tag{46}$$

Then, the discrete input-output relation is expressed as

$$\mathbf{r} = \left(\sum_{p=1}^{P}\sum_{q=-B}^{B} h_p\cdot\mathbf{\Phi}_p\cdot\mathbf{V}^{f_p}\cdot g_q\cdot\mathbf{\Pi}^{\ell_p+q}\right)\cdot\mathbf{s}+\mathbf{w}. \tag{47}$$

Ordering the $P(2B+1)$ tuples (p, q) as $\{(p=1, q=-B), \ldots, (p=1, q=B), (p=2, q=-B), \ldots, (p=P, q=B)\}$,

and defining $u = \{1, \ldots, P(2B+1)\}$ as the corresponding indices, (47) can be rewritten in a final compact form as

$$\mathbf{r} = \left(\sum_{u=1}^{P(2B+1)} h'_u \cdot \mathbf{\Phi}_u \cdot \mathbf{V}^{f_u} \cdot \mathbf{\Pi}^{\ell'_u} \right) \cdot \mathbf{s} + \mathbf{w}, \tag{48}$$

where $h'_u = h_p \cdot g_q$ and $\ell'_u = \ell_p + q$ are defined to highlight the similarity of (48) to the conventional IDID doubly dispersive channel model of (10).

Under this reformulation, it follows that the channel estimation methods that have been previously described for the IDID doubly dispersive channel, can be adapted to the fractional delay and Doppler case, under the new virtual path parameters $\{h'_u, \ell'_u, f_u\}$ for $u = \{1, \ldots, P(2B+1)\}$ and the deterministic structure now available through (15). This shows that AFDM allows accurate estimation of the Doppler shift and delay beyond the Nyquist rate, even though the signal is sampled at the Nyquist rate.

3) SPECIAL CASE: OFDM-LIKE ESTIMATION UNDER LOW DOPPLER

The previous sections presented the channel estimation explicitly in the DAFT domain native to the AFDM, considering fully doubly dispersive channels. However, in condition of low Doppler shift, the latter can be omitted, leading to $\mathbf{V}^{f_p} \approx \mathbf{I}_N$, and then $\mathbf{\Xi}^{\text{OFDM}}$ is diagonal with elements $(\mathbf{\Xi}^{\text{OFDM}})_{n,n} = \sum_{p=1}^{P} h_p e^{-2j\pi \frac{\ell_p n}{N}}$.

Note that these conditions correspond to the channels usually assumed in OFDM systems, so prior OFDM estimation methods remain valid and are especially relevant when only delay estimation is required. It has been shown in [69] that channel estimation can also be performed in the frequency domain using the special cases of AFDM parameters described in [70].

In fact, suppose that $2N\lambda_1 \in \mathbb{Z}$ and $\frac{1}{2\lambda_1} \in \mathbb{Z}$, and that the pilot $\mathbf{x}$ in (39) is now expressed as $\mathbf{x} = [0, .., 0, x_m^{(\text{pil})}, 0, .., 0]^{\mathsf{T}}$. Then, the DFT of the AFDM transmit signal $\mathbf{s}$ in (22), given by

$$\mathbf{z} = \mathbf{F}_N \cdot \mathbf{s} = \mathbf{F}_N \cdot \mathbf{A}^{\mathsf{H}} \cdot \mathbf{x} \in \mathbb{C}^{N \times 1}, \tag{49}$$

has the following regular structure, for $k = \{0, 1, .., N-1\}$,

$$z_k = \begin{cases} \zeta_k \mathbb{1}_{(m-k) \bmod 2N\lambda_1 = 0}, & \text{if } \frac{1}{2\lambda_1} \text{ is even} \\ \zeta_k \mathbb{1}_{\frac{(m-k)}{N\lambda_1} \in \mathbb{Z} \setminus 2\mathbb{Z}}, & \text{if } \frac{1}{2\lambda_1} \text{ is odd,} \end{cases} \tag{50}$$

where $\mathbb{1}_\Omega$ is the indicator function of the elements belonging to the set Ω, and $\mathbb{Z}\setminus 2\mathbb{Z}$ is the subset of $\mathbb{Z}$ corresponding to the odd integers.

Moreover, $\zeta_k \in \mathbb{C}$ is a constant modulus value (*i.e.* $|\zeta_k| = \zeta \in \mathbb{R}$ for any k) whose expression is detailed in [69], with the regular structure of $\mathbf{z}$ illustrated in Fig. 6. It must be noticed that such equispaced pilots in the frequency domain are used in most of the communications standards based on OFDM, in particular, 4G/5G, and WiFi.

Based on this pilot structure using special cases of AFDM parameters, the AFDM demodulation in (26) can be now performed using a DFT matrix $\mathbf{F}_N$ instead of $\mathbf{A}$, which yield

$$\mathbf{y}_{\mathsf{f}} = \mathbf{F}_N \cdot \mathbf{r}$$

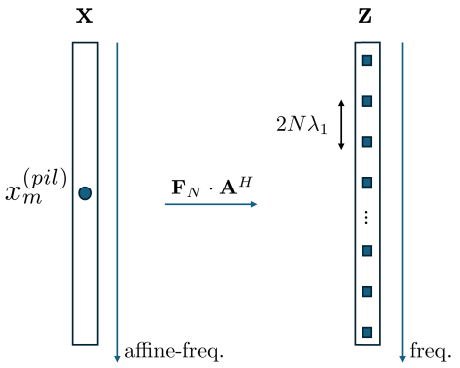

FIGURE 6. Regular structure of $\mathbf{z} = \mathbf{F}_N \cdot \mathbf{A}^{\mathsf{H}} \cdot \mathbf{x}$ where $\mathbf{x} = [0, .., 0, x_m^{(\text{pil})}, 0, .., 0]^{\mathsf{T}}$, in the special cases $2N\lambda_1 \in \mathbb{Z}$ and $\frac{1}{2\lambda_1} \in \mathbb{Z}$.

$$= \underbrace{\mathbf{F}_N \left(\sum_{p=1}^{P} h_p \cdot \mathbf{\Phi}_p \cdot \mathbf{V}^{f_p} \cdot \mathbf{G}(\ell_p) \right) \mathbf{F}_N^{\mathsf{H}}}_{\triangleq \mathbf{\Xi}^{\text{OFDM}} \in \mathbb{C}^{N \times N}} \cdot \mathbf{F}_N \mathbf{A}^{\mathsf{H}} \cdot \mathbf{x} + \mathbf{F}_N \mathbf{w}$$
$$= \mathbf{\Xi}^{\text{OFDM}} \mathbf{z} + \mathbf{F}_N \mathbf{w} \in \mathbb{C}^{N \times 1}, \tag{51}$$

where $\mathbf{\Phi}_p = \mathbf{I}_N$ because $2N\lambda_1 \in \mathbb{Z}$.

The subscript f indicates the received AFDM pilot signal in the frequency domain. In this special case, the usual frequency domain channel estimation used in OFDM [11], [12], [72] can be performed based on (51). Data can also be multiplexed across pilot subcarriers, making AFDM fully backward-compatible with OFDM. Otherwise, in doubly dispersive channels, data can be multiplexed in the affine-frequency domain as previously described in (39) and Fig. 5. Thus, AFDM is flexible: the modulation/demodulation and channel estimation domains and methods can be adapted to the channel severity using a single pilot scheme.

Under the generalized FDFD channel model presented in Section II, the effective channel matrix incorporates inter-sample coupling via the pulse-shaping kernel $\mathbf{G}(\ell_p)$, which affects both pilot footprint and the exploitable sparsity structure. The FDFD model thus provides the structural channel description required to design accurate channel estimators in practical pulse-shaped systems. Further development of dedicated FDFD-aware channel estimation algorithms, including low-complexity schemes that exploit delay-Doppler sparsity in this setting, is addressed in related works such as [73].

C. SIGNAL DETECTION AND RECEIVER ARCHITECTURES

Following the acquisition of channel state information (CSI) via the estimation schemes detailed in the previous section, the receiver must recover the data vector $\mathbf{x}$ from the received affine-frequency domain signal $\mathbf{y}$. The structural insights provided by the generalized FDFD model are also significant in this context, as by reformulating the complex fractional-delay channel into the structured virtual IDID representation as defined in (48), the receiver can use established detection algorithms with well-defined interference cancellation targets. Depending on the interplay between the detector and

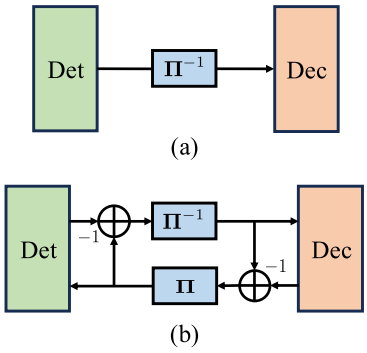

FIGURE 7. Illustration of the AFDM receivers using (a) non-outer iterations and (b) turbo iterations between detectors and decoders.

decoder, AFDM receivers are categorized into two architectures, as illustrated in Fig. 7.

The first category consists of one-shot receivers that perform detection without outer iterations for improved computational efficiency. In contrast, the second category comprises turbo receivers designed for coded AFDM systems, which iteratively exchange extrinsic log-likelihood ratios (LLRs) between the detector and the decoder to approach the channel capacity. We first examine AFDM receiver architectures that operate without outer iterations, then discuss turbo receivers.

1) ONE-SHOT RECEIVERS (NO OUTER ITERATIONS)

The detection algorithms of AFDM receivers fall into two broad groups: linear detectors and sparse channel-enabled detectors.

a) *Linear detectors:* This group comprises zero-forcing (ZF) and linear minimum mean-square error (LMMSE) receivers [35], [74], [75], [76], [77]. Based on the input-output relationship of AFDM in (26), the ZF and minimum mean-square error (MMSE) detectors can be respectively formulated as

$$\tilde{\mathbf{x}}^{\mathrm{ZF}} = \left[(\underline{\boldsymbol{\Xi}}^{\mathrm{AFDM}})^{\mathsf{H}}\underline{\boldsymbol{\Xi}}^{\mathrm{AFDM}}\right]^{-1}(\underline{\boldsymbol{\Xi}}^{\mathrm{AFDM}})^{\mathsf{H}}\mathbf{y}, \tag{52}$$

$$\tilde{\mathbf{x}}^{\mathrm{MMSE}} = \left[(\underline{\boldsymbol{\Xi}}^{\mathrm{AFDM}})^{\mathsf{H}}\underline{\boldsymbol{\Xi}}^{\mathrm{AFDM}} + \sigma_{\mathrm{w}}^2\mathbf{I}_N\right]^{-1}(\underline{\boldsymbol{\Xi}}^{\mathrm{AFDM}})^{\mathsf{H}}\mathbf{y}. \tag{53}$$

The complexity of calculating the MMSE detector directly is on the order of $\mathcal{O}(N^3)$, which is excessive for large-scale AFDM systems. Upon exploiting matrix factorization techniques, such as LU factorization [78], Cholesky decomposition [79], and LDL factorization [80], the complexity of linear detectors can be mitigated. As an example, the LDL factorization-based MMSE detector is elaborated in this section to provide further insight.

LDL factorization-based MMSE detector: Owing to the sparsity pattern of the effective DAFT-domain channel, the matrix $\boldsymbol{\Gamma}$ is Hermitian positive-definite with the lower and upper bandwidth J. Exploiting the banded structure enables the use of an LDL factorization and the trimming matrix $\mathbf{T} = [\mathbf{I}_N]_{Q-(\alpha_{\max}+k_v):N-(\alpha_{\max}+k_v)-1,:}$, where $\boldsymbol{\Gamma}$ is decomposed into a unit lower-triangular matrix $\mathbf{L}$ containing only J sub-diagonals and a diagonal matrix $\mathbf{D}$. This decomposition reduces both memory usage and computational complexity to $\mathcal{O}(J^2N)$, representing a substantial improvement over conventional MMSE inversion.

Once the LDL factors are obtained, the equalization step reduces to solving two triangular systems and one diagonal system, all of which can be efficiently implemented. The complete LDL-based low-complexity MMSE equalization procedure is summarized in **Algorithm 1**.

Algorithm 1 LDL Factorization-Based MMSE Detector

1: Construct $\underline{\boldsymbol{\Xi}}^{\mathrm{AFDM}} = \boldsymbol{\Xi}^{\mathrm{AFDM}}\mathbf{T}^{\mathsf{H}}$.
2: Form the banded matrix $\boldsymbol{\Gamma} = \left(\underline{\boldsymbol{\Xi}}^{\mathrm{AFDM}}\right)^{\mathsf{H}}\underline{\boldsymbol{\Xi}}^{\mathrm{AFDM}} + \sigma_{\mathrm{w}}^2\mathbf{I}_N$.
3: Compute the LDL factorization $\boldsymbol{\Gamma} = \mathbf{L}\mathbf{D}\mathbf{L}^{\mathsf{H}}$, where $\mathbf{L}$ is a lower triangular matrix with J sub-diagonals and $\mathbf{D}$ is diagonal.
4: Solve the lower triangular system $\mathbf{L}\mathbf{f} = \mathbf{y}$.
5: Solve the diagonal system $\mathbf{D}\mathbf{g} = \mathbf{f}$.
6: Solve the upper triangular system $\mathbf{L}^{\mathsf{H}}\mathbf{d} = \mathbf{g}$.
7: Compute the MMSE estimate $\tilde{\mathbf{x}} = (\underline{\boldsymbol{\Xi}}^{\mathrm{AFDM}})^{\mathsf{H}}\mathbf{d}$.

b) *Sparse channel-enabled detectors:* The second group exploits the inherent sparsity of the effective DAFT-domain channel matrix in (26). These detectors adopt low-complexity iterative schemes, including maximal ratio combining (MRC) [21], message passing (MP) [24], [81], [82], [83], and expectation propagation (EP) algorithms [84].

Fig. 8 illustrates an example of the effective channel matrix and its associated factor-graph representation, where each variable node (VN) corresponds to a transmitted symbol and each factor node (FN) represents a received symbol connected to a subset of VNs determined by the channel structure. During message passing, probabilistic information is iteratively exchanged between VNs and FNs to refine the symbol estimates progressively. Next, we provide more details on the MRC and MP detectors, as the main examples.

MRC detector: During the t-th iteration, each symbol $\tilde{x}^{(t)}[n]$ is sequentially updated according to

$$\tilde{x}^{(t)}[n] = \frac{g_n^{(t)}}{d_n + \sigma_{\mathrm{w}}^2}, \tag{54}$$

where

$$g_n^{(t)} = \sum_{l\in\mathcal{L}_n}\left[\underline{\boldsymbol{\Xi}}^{\mathrm{AFDM}}\right]_{l,n}^{*}\Delta^{(t-1)}[l] + d_n\,\tilde{x}^{(t-1)}[n], \tag{55}$$

$$d_n = \sum_{l\in\mathcal{L}_n}\left|\left[\underline{\boldsymbol{\Xi}}^{\mathrm{AFDM}}\right]_{l,n}\right|^2, \tag{56}$$

with $\Delta^{(t-1)}$ denoting the residual vector at the (t–1)-th iteration and $\Delta^{(t-1)}[l]$ as its l-th element, and $\mathcal{L}_n$ represents the set of non-zero row indices in the n-th column of the truncated effective channel $\underline{\boldsymbol{\Xi}}^{\mathrm{AFDM}}$.

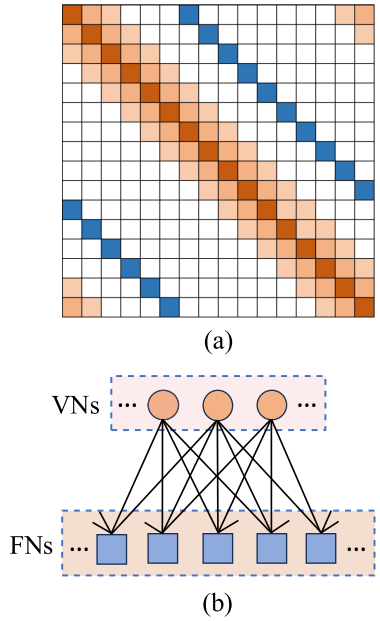

FIGURE 8. Illustration of (a) the effective DAFT-domain channel matrix with two paths and (b) the corresponding factor graph.

After each symbol update, the corresponding residual entries are refined via

$$\Delta^{(t)}[l] = \Delta^{(t-1)}[l] - \left[\underline{\Xi}^{\mathrm{AFDM}}\right]_{l,n}\left(\tilde{x}^{(t)}[n] - \tilde{x}^{(t-1)}[n]\right), \tag{57}$$

for all $l \in \mathcal{L}_n$. Once all symbols have been updated, the refined estimates are used for interference cancellation in the subsequent iteration. This iterative procedure continues until the change between two consecutive symbol vectors becomes negligible or the maximum number of iterations T is reached. These inner iterations are not to be confused with turbo iterations between the detector and decoder, discussed later.

MP detector: From onwards, we assume that the indices ℓ_p and f_p are integer-valued for general $p = \{1, \ldots, P\}$, either for IDID scenarios (10) or following the generalized FDFD model of (48). First, the AFDM input-output relation is rewritten in scalar form as

$$y[a] = \sum_{p=1}^{P} h_p \cdot e^{j\frac{2\pi}{N}\left(Nc_1\ell_p^2 - b\ell_p + Nc_2(b^2-a^2)\right)} \cdot x[b] + \tilde{w}[a], \tag{58}$$

for $a = \{1, \ldots, N\}$. From the vectorized AFDM model in (26), the received vector $\mathbf{y} \in \mathbb{C}^N$ and noise vector $\tilde{\mathbf{w}} \in \mathbb{C}^N$ contain elements $y[a]$ and $\tilde{w}[a]$, respectively. According to (58), the non-zero entries of the effective matrix Ξ^{AFDM} exhibit a structured sparsity pattern: the a-th row contains non-zero elements at indices $(a + \mathrm{loc}_p)_N$, while the non-zero entries of the b-th column appear at indices $(b - \mathrm{loc}_p)_N$.

Then, by letting I_a as the set of non-zero column indices in row a, and D_b as the set of non-zero row indices in column b, the system model (26) naturally corresponds to a sparse factor graph with N VNs representing $\mathbf{x}$ and N FNs representing $\mathbf{y}$. Each observation node $y[a]$ connects to P variable nodes $\{x[b] : b \in I_a\}$, while each variable node $x[b]$ connects to P observation nodes $\{y[a] : a \in D_b\}$.

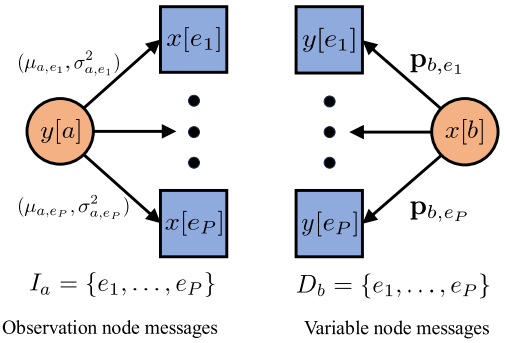

FIGURE 9. The factor graph structure of the MP algorithm.

Directly from (26), the optimal joint maximum a posteriori (MAP) detector is given by

$$\hat{\mathbf{x}} = \arg\max_{\mathbf{x}\in\mathcal{X}^N} \Pr\left(\mathbf{x} \mid \mathbf{y}, \Xi^{\mathrm{AFDM}}\right), \tag{59}$$

but this approach requires exponential complexity in N.

To avoid this complexity, a symbol-wise MAP approximation is adopted as

$$\begin{aligned}\tilde{x}[b] &= \arg\max_{a_j\in\mathcal{X}} \Pr\left(x[b] = a_j \mid \mathbf{y}, \Xi^{\mathrm{AFDM}}\right) \\ &= \arg\max_{a_j\in\mathcal{X}} \frac{1}{M} \Pr\left(\mathbf{y} \mid x[b] = a_j, \Xi^{\mathrm{AFDM}}\right) &\text{(60a)} \\ &\approx \arg\max_{a_j\in\mathcal{X}} \prod_{a\in D_b} \Pr\left(y[a] \mid x[b] = a_j, \Xi^{\mathrm{AFDM}}\right), &\text{(60b)}\end{aligned}$$

where (60a) assumes equiprobable symbols, (60b) uses an independence approximation motivated by the sparsity of Ξ^{AFDM}, and the interference terms $\zeta^{(t)}_{b,a}$ defined in (61) are assumed independent for fixed b.

To address the intractability of the full (60b), an MP detector is employed whose complexity only scales linearly with N. For each observation $y[a]$, the contribution of $x[b]$ is isolated, and the sum of remaining interference terms is approximated as a Gaussian random variable with mean and variance computed in closed form, whose factor is shown in Fig. 9. In the MP framework, observation-to-variable messages consist of these Gaussian parameters, whereas variable-to-observation messages consist of probability mass functions (PMFs) over the constellation alphabet, $\mathbf{p}^{(t)}_{b,a} = \{p^{(t)}_{b,a}(a_j) : a_j \in \mathcal{X}\}$.

Given above, the t-th iteration of the MP algorithm proceeds as follows. First, the interference term $\zeta^{(t)}_{b,a}$ is defined as

$$\zeta^{(t)}_{a,b} = \sum_{e\in D_b, e\neq b} x[e] \cdot \left[\Xi^{\mathrm{AFDM}}\right]_{a,e} + \tilde{w}[a]. \tag{61}$$

Next, the mean $\mu^{(t)}_{a,b}$ and variance $\left(\sigma^{(t)}_{a,b}\right)^2$ are given by

$$\mu^{(t)}_{a,b} = \sum_{e\in I_a, e\neq b} \sum_{j=1}^{M} p^{(t-1)}_{e,a}(a_j) \cdot a_j \cdot \left[\Xi^{\mathrm{AFDM}}\right]_{a,e}, \tag{62}$$

$$\left(\sigma_{a,b}^{(t)}\right)^2 = \sum_{e\in I_a,\, e\neq b}\left(\sum_{j=1}^{M} p_{e,a}^{(t-1)}(a_j)\cdot|a_j|^2\cdot\left|\left[\boldsymbol{\Xi}^{\mathrm{AFDM}}\right]_{a,e}\right|^2 - \left|\sum_{j=1}^{M} p_{e,a}^{(t-1)}(a_j)\cdot a_j\cdot\left[\boldsymbol{\Xi}^{\mathrm{AFDM}}\right]_{a,e}\right|^2\right) + \sigma_{\mathrm{w}}^2. \quad (63)$$

From (58), the corresponding channel coefficient is

$$\left[\boldsymbol{\Xi}^{\mathrm{AFDM}}\right]_{a,e} = h_p\cdot e^{j\frac{2\pi}{N}\left(Nc_1\ell_p^2 - q\ell_p + Nc_2(q^2-a^2)\right)}, \quad (64)$$

where $q = (a+\mathrm{loc}_p)_N$. Then, the updated PMFs are computed as

$$p_{b,a}^{(t)}(a_j) = \Delta\,\tilde{p}_{b,a}^{(t)}(a_j) + (1-\Delta)\,p_{b,a}^{(t-1)}(a_j), \quad (65)$$

where $\Delta\in(0,1]$ is a damping factor, and

$$\tilde{p}_{b,a}^{(t)}(a_j) \propto \prod_{\substack{e\in D_b\\ e\neq a}} \Pr\left(y[e]\mid x[b]=a_j, \boldsymbol{\Xi}^{\mathrm{AFDM}}\right) \quad (66)$$

$$= \prod_{\substack{e\in D_b\\ e\neq a}} \frac{\xi^{(t)}(e,b,j)}{\sum_{m=1}^{M}\xi^{(t)}(e,b,m)}, \quad (67)$$

with

$$\xi^{(t)}(e,b,m) = \exp\left(-\frac{\left|y[e]-\mu_{e,b}^{(t)}-a_m\cdot\left[\boldsymbol{\Xi}^{\mathrm{AFDM}}\right]_{a,e}\right|^2}{(\sigma_{e,b}^{(t)})^2}\right), \quad (68)$$

where the channel coefficient $\left[\boldsymbol{\Xi}^{\mathrm{AFDM}}\right]_{e,b}$ is

$$\left[\boldsymbol{\Xi}^{\mathrm{AFDM}}\right]_{e,b} = h_p\cdot e^{j\frac{2\pi}{N}\left(Nc_1\ell_p^2 - b\ell_p + Nc_2(b^2-u^2)\right)}, \quad (69)$$

with $u = (b-\mathrm{loc}_p)_N$. Then, the symbol estimate is updated as $\tilde{x}[b] = \arg\max_{a_j\in\mathcal{X}} p_b^{(t)}(a_j)$. Within the above steps, convergence is measured as

$$\eta^{(t)} = \frac{1}{N}\sum_{b=1}^{N}\mathbb{I}\left(\max_{a_j\in\mathcal{X}} p_b^{(t)}(a_j)\geq 1-\gamma\right), \quad (70)$$

for a small threshold $\gamma>0$, where

$$p_b^{(t)}(a_j) = \prod_{e\in D_b}\frac{\xi^{(t)}(e,b,j)}{\sum_{m=1}^{M}\xi^{(t)}(e,b,m)}. \quad (71)$$

Finally, the MP detector, as summarized in **Algorithm 2**, terminates when one of the following conditions is met at the end of each iteration: *a)* $\eta^{(t)}=1$; *b)* $\eta^{(t)}<\eta^{(t^*)}-\epsilon$; *c)* $t=T_{\max}$; where t^* is the iteration with the largest $\eta^{(t^*)}$ for $1\leq t^*<t$;

Algorithm 2 MP-Based Detector

Require: Receive signal $\mathbf{y}$ and channel matrix $\boldsymbol{\Xi}^{\mathrm{AFDM}}$.
Preparation: $\mathbf{p}_{b,a}^{(0)} = 1/M$, $b=0,\ldots,N-1$, $a\in D(b)$.
for $t=1$ to $T_{\max}$ **do**
  Observation nodes $y[a]$ compute means $\mu_{a,b}^{(t)}$ and variances $\left(\sigma_{a,b}^{(t)}\right)^2$ via (62) and (63) based on $\mathbf{p}_{b,a}^{(t-1)}$, and pass them to $\{x[b]: b\in I_a\}$.
  Variable nodes $x[b]$ update $\mathbf{p}_{b,a}^{(t-1)}$ via (65), and pass them to $\{y[a]: a\in D_b\}$.
  Calculate convergence indicator $\eta^{(t)}$.
  Update the decision on the transmitted symbols $x[c]$ for $c=1,\ldots,N$, if needed.
  if Stopping criteria are satisfied
  break
end for
return $\hat{\mathbf{x}}$.

2) TURBO RECEIVER

Alternative to the one-shot receivers where there are no outer iterations between the detector and the decoder, AFDM turbo receivers have been investigated in [75], [81], and [85]. As shown in Fig. 7(b), a turbo receiver operates by iteratively exchanging soft reliability information between the detector and the channel decoder, enabling both modules to refine their estimates progressively.

Unlike conventional receivers that perform detection and decoding in isolation, as depicted in Fig. 7(a), a turbo receiver exploits the decoder's soft outputs to help the equalizer suppress residual interference.

Specifically, the extrinsic LLR output by the symbol-to-bit converter (SBC) after the detector can be formulated as [86]

$$L_e(c_{n,j}) = \ln\frac{\sum_{\forall s_i: s_{i,j}=0} p(\hat{x}_n\mid\mathbf{c}_n=\mathbf{s}_i)\prod_{\forall j':j'\neq j} P(c_{n,j'}=s_{i,j'})}{\sum_{\forall s_i: s_{i,j}=1} p(\hat{x}_n\mid\mathbf{c}_n=\mathbf{s}_i)\prod_{\forall j':j'\neq j} P(c_{n,j'}=s_{i,j'})}, \quad (72)$$

where $\hat{x}_n$ denotes the nth estimated element, $\mathbf{c}_n$ is the transmit bit sequence corresponding to x_n, $\mathbf{s}_i$ represents the ith bit pattern associated with the constellation point $a_i\in\mathcal{X}$, and $s_{i,j}$ is the jth bit of $\mathbf{s}_i$.

This iterative feedback loop allows the system to approach optimal joint detection performance with substantially lower computational complexity. A turbo receiver's primary advantage is exploiting coding and diversity gains simultaneously. After each iteration, the improved extrinsic information helps mitigate ICI, reduce error propagation, and reshape the effective channel into a more favorable form for subsequent decoding. This makes turbo receivers effective in highly dispersive environments, where the detector alone is insufficient, at the cost of the additional complexity and latency of the outer iterations.

In summary, while the distinct matrix structure of AFDM necessitates specialized internal detection logic, such as LDL-based banded equalization or sparse factor-graph processing, the high-level architectural principles remain consistent with legacy OFDM receivers. Therefore, moving from OFDM to AFDM receivers primarily involves replacing the core detection block, while the surrounding infrastructure remains unchanged. This compatibility ensures that the extensive ecosystem of receiver optimization techniques developed for 5G can be directly extended to AFDM, providing a practically viable evolutionary path for 6G.

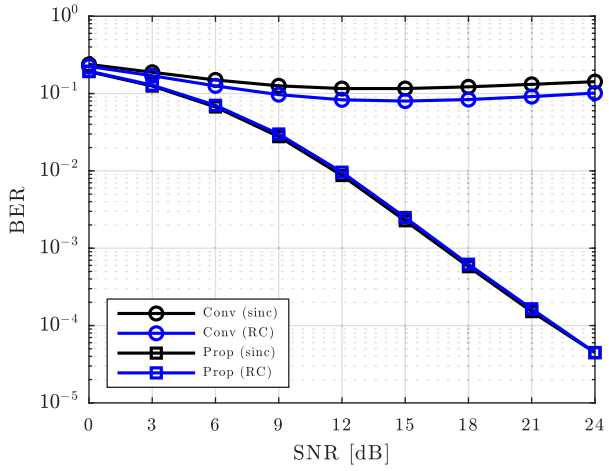

FIGURE 10. Uncoded AFDM-QPSK BER over a true FDFD channel (N=64, P=3), comparing genie-MMSE receivers built on the *proposed* FDFD model (fractional-delay) vs. the IDFD (integer-delay) model.

D. IMPACT OF FRACTIONAL-DELAY MODEL ON RECEIVER DESIGN

The generalized FDFD model of Section II-C carries concrete consequences for receiver design, which we quantify here along two axes of detection performance and detector complexity.

We consider AFDM with quadrature phase shift keying (QPSK) over a true FDFD channel ($N = 64$, $P = 3$, fractional delays ℓ_p and Doppler f_p), and compare two genie-aided MMSE receivers given perfect knowledge of the path parameters (h_p, ℓ_p, f_p) that equalize the same received vector, differing only in the channel model used to construct the equalizer. Namely, the *proposed* model uses the exact FDFD effective channel $\mathbf{AHA}^{\mathsf{H}}$ with $\mathbf{H}$ from (14)–(17), whereas the *conventional* model rounds the delays to the integer grid $(\ell_p \to \lfloor \ell_p \rceil)$, i.e., the standard IDFD assumption that neglects inter-sample coupling.

Fig. 10 shows that the conventional integer-delay receiver exhibits an irreducible bit error rate (BER) floor at 10^{-1} *even with perfect parameter knowledge*, because the integer-tap model structurally cannot represent fractional-delay inter-sample coupling. The receiver built on the proposed FDFD model removes this floor and recovers the expected waterfall. This isolates the practical necessity of the FDFD model: ignoring fractional delay induces a *modeling* error rather than an estimation error, and it dominates performance at moderate-to-high SNR regimes.

In addition, the same fractional-delay coupling governs the *sparsity* of the effective channel matrix, and hence the cost of the sparse detectors discussed in the previous sections. Quantifying the channel-matrix density visualized in Fig. 2 as the average number of taps per row capturing 99% of the row energy (over random FDFD realizations, $N = 64$, $P = 3$), we obtain 2.6 (rectangular), 4.6 (raised cosine, $\alpha = 0.5$), and 12.3 (sinc) taps per row. As the per-iteration cost of message-passing and banded MMSE detectors scales with the number of nonzero taps per row, the transmit pulse directly trades spectral containment against detector complexity: the ideal band-limited (sinc) pulse maximizes inter-sample coupling and detector load, the rectangular pulse minimizes both (at the cost of spectral leakage), and a practical raised-cosine pulse offers a favorable compromise.

E. EXTENSION TO MIMO-AFDM SYSTEMS

The SISO channel estimation and detection methods of Sections IV-B and IV-C extend directly to MIMO-AFDM via the per-antenna model of (28): distributing pilots across transmit antennas as in (39) allows the $N_{\mathrm{r}} \cdot N_{\mathrm{t}}$ channels to be estimated using the same SISO techniques applied per receive antenna, following the principle established in [87] and closely related to the multiple pilot-aided estimation of [66]. When the Doppler shift is small enough to be neglected, as in conventional OFDM systems, digital beamforming (precoding in downlink (DL) or combining in uplink (UL)) can further be performed per-subcarrier in the frequency domain [88], yielding

$$\mathbf{y}_{\mathrm{f},k} = \mathbf{\Xi}_k^{\mathrm{OFDM}} \mathbf{z}_k + \mathbf{w}_{\mathrm{f},k} \in \mathbb{C}^{N_{\mathrm{r}} \times 1}, \tag{73}$$

where $\mathbf{z}_k \in \mathbb{C}^{N_{\mathrm{t}} \times 1}$ is the per-subcarrier transmitted symbol vector across antennas and $\mathbf{\Xi}_k^{\mathrm{OFDM}} \in \mathbb{C}^{N_{\mathrm{r}} \times N_{\mathrm{t}}}$ denotes the corresponding diagonal-Doppler channel matrix, onto which standard MIMO-OFDM beamforming techniques (e.g., zero-forcing) apply directly. Additionally, in the special cases of AFDM parameters [70] where $2N\lambda_1 \in \mathbb{Z}$ and $\frac{1}{2\lambda_1} \in \mathbb{Z}$, channel estimation and beamforming can be performed in the frequency domain, as described in Section IV-B.3.

F. MULTIPLE ACCESS AND COEXISTENCE WITH OFDM

The flexibility and backward compatibility of AFDM make it well suited to efficient, resilient multiple access in complex electromagnetic environments. Specifically, one can configure c_1 for different users based on their moving speeds to achieve robust transmissions. This supports multiuser communications in, e.g., 6G NTNs, where base stations (e.g., high-altitude platform stations and low-earth-orbit satellites) and user terminals (e.g., flying drones, connected vehicles, high-speed trains) move at varying speeds. The waveform coexistence between AFDM and OFDM was studied in [89], revealing that each waveform admits a sparse, comb-like representation in the other's native domain. By exploiting the full diversity property of AFDM, a rate-splitting multiple access (RSMA) framework was reported in [90], in which the coexistence between AFDM and OFDM was investigated. A downlink AFDM-RSMA scheme was proposed in [91] with the key idea that private messages of different users are mapped onto orthogonal chirps, while common messages span all the chirps. To support massive connectivity over high mobility channels, the integration of AFDM and sparse code multiple access (SCMA), called AFDM-SCMA, was studied in [81]. As a code-domain non-orthogonal multiple access scheme [81], OFDM-based SCMA can degrade under carrier frequency offsets [92] or Doppler shifts. AFDM-SCMA

was shown to achieve favorable error-rate performance by combining the strengths of both techniques.

A complementary multiple access paradigm is DAFT-spreading-based affine frequency division multiple access (AFDMA) [93], which spreads each user's data across the full DAFT domain rather than allocating distinct subcarrier or block segments. This approach exploits the full diversity and spreading gain of the DAFT basis to improve robustness in high-mobility environments, and can be contrasted with the per-block and per-subcarrier multiplexing schemes described below in terms of spectral efficiency, receiver complexity, and diversity exploitation.

1) GENERAL AFDMA AND COEXISTENCE WITH OFDMA

Two distinct paradigms may facilitate AFDMA, as illustrated in Fig. 11: *a)* per-block multiplexing and *b)* per-subcarrier multiplexing. These schemes enable multiple user equipments (UEs) to share the available bandwidth while maintaining compatibility with legacy orthogonal frequency division multiple access (OFDMA) systems.

a: PER-BLOCK AFDMA

In the per-block approach, K_{UE} users share a total bandwidth of N subcarriers, and each user $k_{\mathrm{UE}} \in \{1, \ldots, K_{\mathrm{UE}}\}$ is allocated $N_{k_{\mathrm{UE}}}$ subcarriers such that $N = \sum_{k_{\mathrm{UE}}=1}^{K_{\mathrm{UE}}} N_{k_{\mathrm{UE}}}$. The composite transmit signal is expressed as

$$\mathbf{s} = \mathbf{F}_N^{\mathsf{H}} \cdot \left[(\mathbf{F}_{N_1} \mathbf{s}_1)^{\mathsf{T}}, \ldots, (\mathbf{F}_{N_{K_{\mathrm{UE}}}} \mathbf{s}_{K_{\mathrm{UE}}})^{\mathsf{T}} \right]^{\mathsf{T}}, \tag{74}$$

where $\mathbf{s}_{k_{\mathrm{UE}}} = \mathbf{A}_{k_{\mathrm{UE}}}^{\mathsf{H}} \mathbf{x}_{k_{\mathrm{UE}}} \in \mathbb{C}^{N_{k_{\mathrm{UE}}} \times 1}$ represents the chirped sub-signal of the k_{UE}-th user.

At the receiver, the composite signal is decomposed in the frequency domain via an N-point DFT $\mathbf{F}_N$, after which the individual user signals are recovered using UE-specific AFDM demodulation matrices. Given the above, a primary advantage of per-block AFDMA is its native support for coexistence between AFDM and OFDM. Since the sub-signals are orthogonal in the frequency domain, an AFDM sub-block can be replaced by an OFDM sub-block ($\mathbf{x}_{k_{\mathrm{UE}}}$) without inducing inter-carrier interference, allowing for transparent spectral sharing between the two waveforms.

b: PER-SUBCARRIER AFDMA

As an alternative, per-subcarrier AFDMA uses specific AFDM parameter configurations where $2N\lambda_1 \in \mathbb{Z}$ and $1/(2\lambda_1) \in \mathbb{Z}$, as discussed in Section IV-B.3. Under these conditions, a data element mapped to an affine-frequency index m is spread across specific frequency-domain indices k satisfying $(k)_{2N\lambda_1} = (m)_{2N\lambda_1}$. By allocating subcarriers with index $(m)_{2N\lambda_1} = r$ to a given user, up to $K_{\mathrm{UE}} = 2N\lambda_1$ users can be multiplexed. The transmit signal is given by

$$\mathbf{s} = \mathbf{A}^{\mathsf{H}} \cdot \sum_{k_{\mathrm{UE}}=0}^{2N\lambda_1 - 1} \mathbf{x}_{k_{\mathrm{UE}}}, \tag{75}$$

where $\mathbf{x}_{k_{\mathrm{UE}}}$ contains non-zero symbols only at indices $k_{\mathrm{UE}} + n(2N\lambda_1)$.

Unlike the per-block approach, per-subcarrier AFDMA ensures subcarrier orthogonality in both the affine-frequency and frequency domains. This allows for fine-grained multiplexing of AFDM and OFDM symbols within the same block, as

$$\mathbf{s} = \mathbf{A}^{\mathsf{H}} \cdot \sum_{k_{\mathrm{UE}} \neq i}^{2N\lambda_1 - 1} \mathbf{x}_{k_{\mathrm{UE}}} + \mathbf{F}^{\mathsf{H}} \mathbf{x}_i, \tag{76}$$

where user i utilizes OFDM.

The resulting hybrid signal is easily separable at the receiver, facilitating flexible multi-user access under coexisting OFDM and AFDM signaling.

2) MIMO-AFDMA

Building on the extension of AFDM to MIMO systems and the multi-user frameworks of legacy MIMO-OFDM, we consider its adaptation to multi-user MIMO, referred to as MIMO-AFDMA. MIMO-AFDMA further extends multi-user capabilities by enabling simultaneous communication between a base station and multiple UEs through spatial and domain-specific multiplexing, as illustrated in Fig. 12. We present a general overview of MIMO-AFDMA operation in both the DL and UL.

In the DL, with $N_{\mathrm{r}} \geq K_{\mathrm{UE}}$, the first $(Q+1)N_{\mathrm{r}}$ indices of each transmit vector $\mathbf{x}_{n_{\mathrm{t}}}$ are reserved for pilot symbols to

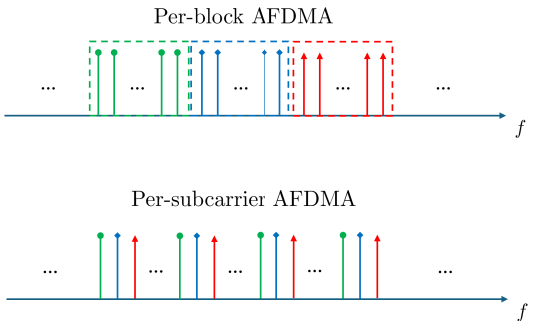

FIGURE 11. Frequency mapping strategies for AFDMA: per-block (top) and per-subcarrier (bottom) approaches.

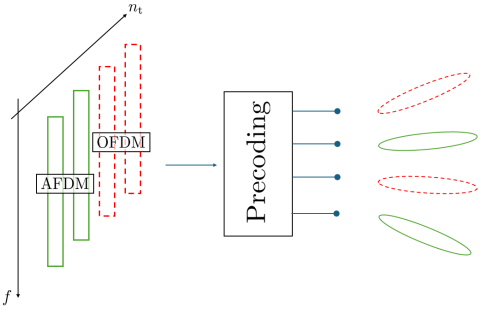

FIGURE 12. Spatial coexistence in MIMO-AFDM systems utilizing digital beamforming ($N_{\mathrm{t}} = 4$).

facilitate channel acquisition. The remaining indices are used for data, formatted as

$$\mathbf{x}_{n_t} = [\underbrace{0,\ldots,0}_{(Q+1)N_r},\underbrace{0,\ldots,0}_{Q},\mathbf{x}_d^{(0)},\ldots,\underbrace{0,\ldots,0}_{Q},\mathbf{x}_d^{(K_{UE}-1)}]^T, \quad (77)$$

where $\mathbf{x}_d^{(k_{UE})}$ represents the data payload for the k_{UE}-th user.

Each data block is isolated by guard bands of Q zero samples to prevent inter-user interference at the receiver. Since all transmit antennas broadcast the data blocks, users can exploit spatial diversity to improve detection reliability.

In the UL, the N available subcarriers are divided into subsets of contiguous subcarriers allocated to individual UEs based on throughput requirements. Each UE transmits its specific payload $\mathbf{x}_{k_{UE}}$, consisting of an embedded pilot and the data block $\mathbf{x}_d^{(k_{UE})}$. This domain partitioning ensures that multiple users can transmit asynchronously in high-mobility environments while minimizing mutual interference, thanks to AFDM's intrinsic Doppler robustness.

AFDM and OFDM signals can also be spatially multiplexed without interference, as illustrated in Fig. 12 where $n_t = 4$ and two UEs use OFDM. Mathematically, it corresponds to the multiplexing of AFDM and OFDM data within $\mathbf{z}_k$ in (73). This again demonstrates AFDM/OFDM coexistence within one system and AFDM's backward compatibility with OFDM, particularly at low Doppler.

G. PHASE NOISE AND CARRIER FREQUENCY OFFSET

Phase noise (PHN) and carrier frequency offset (CFO) are two primary hardware impairments arising from the non-idealities of practical local oscillators (LOs) [94]. In modern broadband systems, especially those operating at higher carrier frequencies, LOs are susceptible to thermal and flicker noise-induced instabilities. These imperfections manifest as random phase drifts and frequency deviations that distort the baseband waveform during up- and down-conversion. While these effects are highly detrimental to OFDM, which relies on precise time-frequency alignment, the chirped subcarriers of AFDM offer an inherent structural resilience to these distortions [95].

1) CHARACTERIZATION OF PHN AND CFO

To characterize the statistical behavior of PHN, a discrete-time Wiener process model is typically employed [96]. In this framework, the Gaussian PHN increments $\Delta[n]$ at a given antenna evolve as

$$\varphi[n] = \varphi[n-1] + \Delta[n],\ n = 1,\ldots,N-1, \quad (78)$$

where $\Delta[n]$ is a zero-mean Gaussian process with variance $\sigma_\Delta^2 = 4\pi^2 f_c^2 \xi T_s$, and ξ represents the oscillator quality and T_s denotes the sampling period [97].

Given the above, the resulting distortion is modeled by the diagonal PHN matrix as

$$\mathbf{\Theta} = \mathrm{diag}\left\{e^{j\varphi[0]},\ldots,e^{j\varphi[N-1]}\right\}. \quad (79)$$

The spatial correlation of PHN is determined by the LO architecture. In co-located MIMO arrays, a common local oscillator (CLO) is typically utilized, resulting in identical PHN across all antenna elements. Conversely, distributed or RF-chain-per-antenna architectures employ separate local oscillators (SLOs), leading to spatially independent phase fluctuations. This distinction is critical, as CLO induces coherent distortion, whereas SLOs can significantly degrade beamforming gains and the accuracy of spatial parameter estimation [98].

CFO arises from frequency mismatches between the transmit and receive LOs, which are inevitable due to hardware tolerances and temperature variations. This mismatch induces a linearly increasing phase rotation across the time-domain samples. In multi-carrier systems, this destroys subcarrier orthogonality, leading to severe ICI. For chirp-based AFDM, CFO manifests as an additional Doppler-like phase rotation, characterized by the diagonal matrix [45], [92]

$$\mathbf{P} = \mathrm{diag}\left\{1, e^{j2\pi\theta_{CFO}/N},\ldots,e^{j2\pi\theta_{CFO}(N-1)/N}\right\}, \quad (80)$$

where θ_{CFO} represents the normalized CFO factor.

In all, incorporating the impairments, the effective channel matrix from (48) is generalized as

$$\mathbf{H} = \mathbf{\Theta P}\left(\sum_{p=1}^{P} h_p \cdot \mathbf{\Phi}_p \cdot \mathbf{V}^{f_p} \cdot \mathbf{\Pi}^{\ell_p}\right). \quad (81)$$

2) WAVEFORM RESILIENCE AND PERFORMANCE

The impact of PHN and CFO differs fundamentally between the two waveforms due to their distinct basis functions. In OFDM, these impairments disrupt the frequency-domain orthogonality, manifesting as a common phase error (CPE) and rapidly varying ICI that scales with the magnitude of the CFO. Consequently, OFDM requires highly accurate tracking and compensation to prevent BER degradation.

In contrast, AFDM utilizes DAFT-domain chirps that sweep across the time-frequency plane. This structure provides frequency diversity, as the symbol energy is spread across multiple frequency components. The phase rotation induced by CFO partially aligns with the intrinsic linear chirp slope, rendering AFDM significantly more tolerant to moderate CFO levels compared to the static sinusoidal subcarriers of the conventional OFDM.

Numerical evaluations of BER performance, as shown in Fig. 13, confirm these characteristics. Using $N = 128$ subcarriers, QPSK modulation, and $\theta_{CFO} = 0.1$, it is observed that AFDM performance remains nearly identical to the ideal (impairment-free) case. Conversely, at a BER of 3×10^{-3}, OFDM exhibits signal-to-noise ratio (SNR) losses of approximately 2 dB due to PHN and 8 dB due to CFO. Furthermore, in PHN scenarios at a BER of 10^{-3}, AFDM achieves a gain of 10.5 dB over OFDM, consistent with improved robustness to oscillator non-idealities.

H. DEGREES OF FREEDOM VIA THE CHIRP PARAMETER DOMAIN

The parameterizable nature of the DAFT, in its two chirp parameters λ_1 and λ_2, allows AFDM to adapt its signal

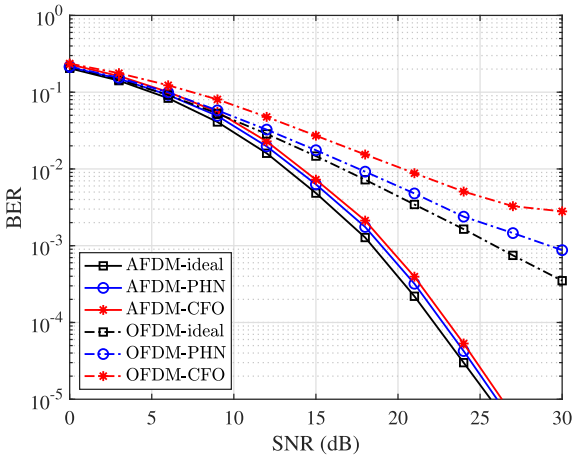

FIGURE 13. BER performance of OFDM/AFDM under PHN and CFO impairments ($N=128$, QPSK, $\theta_{\text{CFO}}=\frac{1}{10}$, $P=3$), with LMMSE detection.

structure to specific system requirements beyond conventional data transmission. In addition to tuning the parameters for robustness and diversity, this flexibility can also be exploited to implement functionalities such as index modulation (IM), physical layer security (PLS), and PAPR reduction.

It is essential to note that these functionalities can be implemented without altering the fundamental AFDM framework, preserving its structural compatibility with the OFDM legacy; OFDM and OTFS lack an analogous continuously tunable chirp-rate parameter that enables this without dedicated structural modification.

1) INDEX MODULATION

IM schemes originally proposed for OFDM [99], [100] have also been effectively adapted to the AFDM framework [24], [101]. Recent works have further extended the AFDM-IM framework with new index dimension designs and enhanced spectral efficiency [27], [28]. This technique involves partitioning N subcarriers into K_{IM} subsets, each containing $N_{\text{IM}}=\frac{N}{K_{\text{IM}}}$ subcarriers, and in each subset, $m_{\text{IM}}<N_{\text{IM}}$ subcarriers are selected as active, while the remaining $N_{\text{IM}}-m_{\text{IM}}$ indices are left inactive. Consequently, binary information is conveyed not only through the M-ary complex symbols but also through the selection of active indices, as also extensively studied in other IM literature such as spatial modulation (SM) [102], [103], [104] and STSK [105] for MIMO systems. More recently, by using additional bits to select the active transmit antennas, the GSM-aided AFDM scheme has been studied in [76].

The IM spectral efficiency (in bps) is given by

$$R_{\text{IM}}=K_{\text{IM}}\cdot\log_2\left(\left\lfloor\binom{N_{\text{IM}}}{m_{\text{IM}}}\right\rfloor\right)+K_{\text{IM}}m_{\text{IM}}\cdot\log_2(M), \quad (82)$$

offering improved BER performance or spectral efficiency compared to standard AFDM [106].

From a structural perspective, AFDM-IM represents an evolution of OFDM-IM where the modulation is performed in the DAFT domain rather than the frequency domain. This backward compatibility allows the adaptation of various OFDM-IM enhancements, such as subcarrier power modulation [107] and multi-mode signaling [108], [109].

Beyond standard subcarrier selection, AFDM introduces unique dimensions for IM through its parameterizable chirp structure. For instance, the chirp parameter λ_2 can be dynamically selected from a finite set for each subcarrier subset, effectively increasing the aggregate bit rate without requiring additional bandwidth [25].

Alternatively, information can be conveyed via the permutation of the chirp sequences themselves, a technique known as *chirp-permutation* IM (CP-IM) [26], [110]. This approach has been shown to provide significant performance gains while maintaining a complete set of active subcarriers, thereby avoiding the spectral efficiency loss typically associated with traditional IM schemes.

2) PHYSICAL LAYER SECURITY

PLS uses the physical dimensions of the communication system, such as time, frequency, and chirp parameters, to complement higher-layer encryption. AFDM offers a unique paradigm for PLS centered on the tunability of (λ_1,λ_2). Research indicates that AFDM can achieve strong physical-layer security by utilizing permutations over chirp sequences [31], [110], creating a combinatorial complexity that remains resilient even against quantum-accelerated eavesdropping attempts. In addition, analytical results also demonstrate that AFDM provides higher PLS compared to OTFS and OFDM, as measured by the brute-force complexity required for unauthorized demodulation [29]. Furthermore, parameter-hopping schemes for (λ_1,λ_2) can be implemented to dynamically vary the waveform characteristics [30]. Combined with its structural robustness against jamming and eavesdropping due to its wideband chirp nature [29], [111], AFDM offers enhanced physical-layer security.

3) PAPR REDUCTION

As AFDM is constructed from a summation of subcarriers, it exhibits a PAPR profile statistically similar to that of OFDM, whereas OTFS typically achieves lower values [20], [110]. However, this similarity is a significant advantage for system reusability. Legacy OFDM PAPR reduction techniques such as clipping, μ-law companding [112], and data precoding [113] are directly applicable to AFDM, allowing for the reuse of established hardware infrastructure, including PA linearization and digital front-end processing.

Beyond legacy methods, specific AFDM PAPR reduction strategies have recently emerged. These include pre-chirp selection, where λ_2 is optimized within a finite set to minimize the peak power for each block [114], and the use of block-diagonal DFTs pre-chirp matrices [115].

To complement the per-aspect discussions throughout this section, Table 2 consolidates the key characteristics of OFDM, AFDM, and OTFS into a single at-a-glance comparison spanning various aspects of the OFDM-based

TABLE 2. Consolidated Qualitative Comparison of OFDM, AFDM, and OTFS Across Key Implementation and Performance-Related Aspects.

Aspect	OFDM	AFDM	OTFS
Core transform	N-point IFFT/FFT	N-point IFFT/FFT + two 1D chirp rotations	ISFFT + pulse-shaped HT (or IDZT + 2D DD processing)
Modulator complexity	$5N\log_2 N$ [FLOPS]	$5N\log_2 N + 12N$ [FLOPS]	$5N\log_2 N + 5N\log_2 L + 2N$ [FLOPS]
FFT-size flexibility	Arbitrary N	Arbitrary N	Constrained to $N = KL$
Pulse shaping	1D time-domain	1D time-domain	1D time-domain prototype pulse (pulse-shaped HT), or 2D DD-domain convolution (Zak-OTFS)
Prefix	Cyclic prefix (CP)	Chirp-periodic prefix (CPP), same length as CP	Per-frame ZP/CP (rectangular pulses); double time–frequency CP under practical pulse shaping [65]
Resource grid	1D time-frequency	1D time-frequency	2D delay-Doppler grid
Channel estimation & pilot overhead	1D pilots, low overhead	1D chirp-aware pilots, comparable overhead	2D DD pilots with 2D guard regions, higher overhead
Doppler robustness & diversity	Low; loses subcarrier orthogonality	High; attains full delay-Doppler diversity	High; asymptotic diversity order one when uncoded (ML detection); full delay-Doppler diversity via phase-rotation precoding, with near-full-diversity slopes at practical SNR [44]
PHN & CFO resilience	Baseline	Improved; PHN gain and reduced CFO-induced SNR loss vs. OFDM, demonstrated in Fig. 13	Improved; robust to CFO/Doppler-induced ICI; more PHN-resilient than OFDM [116], [117]
PAPR	High; Baseline	High; Statistically identical to OFDM	Lower than OFDM/AFDM
Baseband PHY reuse & standardization	Native baseline	High; implemented as a wrapper around OFDM baseband blocks	Medium; OFDM FFT core reusable (fully so under rectangular pulses), but the 2D delay-Doppler grid, pilots, and estimation/equalization require reformulation of PHY processing blocks (see Table 3)

TABLE 3. Reusability Analysis: AFDM Against the OFDM Legacy Infrastructure.

Domain	Module / Function	AFDM	OTFS	Architectural Impact & Rationale
RF & Analog	RF Chain *(PA, Antennas, Cabling)*	**Direct Reuse**	**Direct Reuse**	AFDM retains the statistical PAPR distribution and spectral mask of OFDM. No new power back-off, PA linearization, or antenna/cable redesign is required. OTFS likewise reuses the RF front-end, and typically exhibits a lower PAPR.
	Mixed Signal *(ADC / DAC)*	**Direct Reuse**	**Direct Reuse**	Sampling rates, quantization noise floors, and dynamic range requirements remain identical to OFDM for both AFDM and OTFS.
PHY Layer	FFT / IFFT Engines	**Direct Reuse**	**Direct Reuse**	The core butterfly accelerators are preserved. AFDM is implemented as a wrapper around the legacy OFDM block, and OTFS can also reuse the core FFT but of multiple stages.
	Full Pulse-Shaped Waveform Generation	**Soft Update**	**Logic Update**	AFDM requires insertion of two element-wise phase rotation vectors digitally (pre/post-chirp) at $\mathcal{O}(N)$ complexity, whereas OTFS requires multi-stage 2D transform and delay-Doppler pulse-shaping processing.
	Channel Estimation / Equalization	**Logic Update**	**Logic Update**	Requires new algorithms for the additional Doppler-domain recovery and equalization (in DAFT domain). Standard estimators (LS/MMSE) must be upgraded, or alternate novel estimators can be used. OTFS similarly requires 2D delay-Doppler estimation and equalization.
	Pilot Structure	**Adaptable**	**Logic Update**	Legacy one-dimensional time-domain pilot placement and padding are reusable for AFDM, but optimal performance in high mobility may require different placement within and chirp-aware wrapping. OTFS requires dedicated 2D delay-Doppler pilots with 2D guard regions.
MAC & Control	Resource Grid	**Compatible**	**Logic Update**	Resources map to 1D streams. The fundamental time-frequency resource element (RE) grid structure is preserved for AFDM, whereas OTFS operates on a 2D delay-Doppler grid constrained to $N = KL$.
	Control Signaling (DCI)	**Extension**	**Extension**	Standard downlink control information (DCI) formats can apply, but new chirp parameters (chirp indices) may require additional signaling bits for AFDM, and OTFS requires grid configuration information.

standardization roadmap. The comparison is qualitative and intended to summarize the structural and implementation-level relationships established in this article. Detailed performance comparisons among delay-Doppler waveforms are available in dedicated studies [20], [41], [42].

I. REUSABILITY OF AFDM: A LAYER-BY-LAYER SUMMARY

To consolidate the preceding technical analysis, this subsection qualitatively evaluates the reusability of AFDM with the established OFDM legacy. This assessment matters for

6G standardization, where minimizing infrastructure replacement costs is as important as performance gains. A detailed breakdown of this compatibility is presented in Table 3. In the **RF and Analog** domain, the waveform's statistical similarity to OFDM allows for the direct reuse of PAs and transceivers without redesign. In the **PHY Layer**, while the core FFT hardware accelerators are preserved, the transition mainly requires software updates for channel estimation logic and phase rotation (chirping). Finally, **MAC** compatibility is achieved through minimal extensions to existing structure and control signaling.

V. OPEN RESEARCH CHALLENGES AND CONCLUSION

While the preceding analysis establishes the compatibility and backward reusability of AFDM relative to the OFDM legacy, several practical aspects remain open, which we briefly summarize below.

Synchronization: The chirped subcarrier structure alters AFDM's sensitivity to residual timing and frequency offsets relative to OFDM. While Section IV characterizes steady-state PHN/CFO impairment, low-overhead acquisition and tracking loops that are robust to joint delay-Doppler dispersion remain immature, and whether legacy OFDM synchronization circuitry can be reused with only chirp-aware post-processing or dedicated estimators are required remains an open question.

Channel estimation overhead and FDFD-aware frameworks: This article assumes perfect channel state information to isolate the effective channel's structural properties from estimation artifacts. Under the generalized FDFD model, however, the effective channel is no longer strictly sparse, and pulse-shaping-induced inter-sample coupling increases the support an estimator must resolve. Therefore, quantifying the resulting pilot overhead and designing dedicated FDFD-aware estimators are substantial directions, as reflected in growing related interest [73].

Standardization pathway: Table 3 suggests that AFDM can be integrated with limited modification to the OFDM physical layer, but control-plane implications remain unspecified. For example, exact signaling of chirp parameters, coexistence of AFDM/OFDM numerologies on a shared resource grid, and alignment with ongoing 3GPP 6G waveform study items [3], [5] are concrete open items.

VI. CONCLUSION

Overall, we highlighted that AFDM is a well-positioned waveform candidate for 6G+ wireless systems, bridging extreme-mobility performance requirements and the practical demand for hardware reusability. Built upon the established OFDM legacy, AFDM achieves high-fidelity communications in doubly dispersive channels through a modular, evolutionary approach rather than a radical system redesign. The presented analysis confirms extensive reusability in the RF front-end and the receiver's FFT/IFFT core, while channel estimation and equalization require logic-level updates, as summarized in Table 3. The tunable chirp-parameter domain further offers degrees of freedom for secondary functionalities, including IM, PLS, and sensing, while maintaining compatibility with legacy resources. AFDM thus offers a practically viable waveform candidate for 6G standardization and beyond, preserving prior engineering investments while meeting the demands of future wireless systems.

VII. USE OF AI TOOLS

Generative AI tools, including ChatGPT, Gemini, Claude, and Copilot, were utilized in this work for editorial refinement, code optimization, and literature scoping. These tools served only as auxiliary instruments to enhance clarity and presentation, and they did not generate new scientific concepts or results. The authors have carefully verified all AI-assisted content and assume full responsibility for the accuracy, integrity, and originality of the manuscript.

REFERENCES

[1] W. Jiang, B. Han, M. A. Habibi, and H. D. Schotten, "The road towards 6G: A comprehensive survey," *IEEE Open J. Commun. Soc.*, vol. 2, pp. 334–366, 2021.

[2] C.-X. Wang et al., "On the road to 6G: Visions, requirements, key technologies, and testbeds," *IEEE Commun. Surveys Tuts.*, vol. 25, no. 2, pp. 905–974, 2nd Quart. 2023.

[3] *Feature Lead Summary #3 on 6G Waveform (Source: Nokia), RAN1 Meeting #122bis*, document TSG RAN, R1-2508043, 3GPP, Oct. 2025.

[4] *Study on 6G Use Cases and Service Requirements*, document TR 22.870, 3GPP, Jun. 2025.

[5] *New SID: Study on 6G Radio, document TSG RAN*, RP-251881, 3GPP, RAN Meeting #108., Jun. 2025.

[6] E. Dahlman, S. Parkvall, and J. Skold, *5G NR: The Next Generation Wireless Access Technology*. New York, NY, USA: Academic, 2020.

[7] *Evolved Universal Terrestrial Radio Access (E-UTRA); Physical Channels and Modulation*, document TS 36.211, 3GPP, 2008.

[8] *NR; Physical Channels and Modulation*, document TS 38.211, 3rd Generation Partnership Project (3GPP), Release 15, 2018.

[9] M. Morelli, C.-C.-J. Kuo, and M.-O. Pun, "Synchronization techniques for orthogonal frequency division multiple access (OFDMA): A tutorial review," *Proc. IEEE*, vol. 95, no. 7, pp. 1394–1427, Jul. 2007.

[10] S. H. Han and J. H. Lee, "An overview of peak-to-average power ratio (PAPR) reduction techniques for multicarrier transmission," *IEEE Wireless Commun.*, vol. 12, no. 2, pp. 56–65, Apr. 2005.

[11] M. K. Ozdemir and H. Arslan, "Channel estimation for wireless OFDM systems," *IEEE Commun. Surveys Tuts.*, vol. 9, no. 2, pp. 18–48, 2nd Quart., 2007.

[12] Y. Liu, Z. Tan, H. Hu, L. J. Cimini, and G. Y. Li, "Channel estimation for OFDM," *IEEE Commun. Surveys Tuts.*, vol. 16, no. 4, pp. 1891–1908, 4th Quart., 2014.

[13] W. Saad, M. Bennis, and M. Chen, "A vision of 6G wireless systems: Applications, trends, technologies, and open research problems," *IEEE Netw.*, vol. 34, no. 3, pp. 134–142, May 2020.

[14] D. Bliss and S. Govindasamy, *Adaptive Wireless Communications: MIMO Channels and Networks*. Cambridge, U.K.: Cambridge Univ. Press, 2013.

[15] V. Koivunen, M. F. Keskin, H. Wymeersch, M. Valkama, and N. González-Prelcic, "Multicarrier ISAC: Advances in waveform design, signal processing, and learning under nonidealities," *IEEE Signal Process. Mag.*, vol. 41, no. 5, pp. 17–30, Sep. 2024.

[16] G. Araniti, A. Iera, S. Pizzi, and F. Rinaldi, "Toward 6G non-terrestrial networks," *IEEE Netw.*, vol. 36, no. 1, pp. 113–120, Jan. 2022.

[17] M. Noor-A-Rahim et al., "6G for vehicle-to-everything (V2X) communications: Enabling technologies, challenges, and opportunities," *Proc. IEEE*, vol. 110, no. 6, pp. 712–734, Jun. 2022.

[18] T. Wang, J. G. Proakis, E. Masry, and J. R. Zeidler, "Performance degradation of OFDM systems due to Doppler spreading," *IEEE Trans. Wireless Commun.*, vol. 5, no. 6, pp. 1422–1432, Jun. 2006.

[19] F. Liu et al., "Integrated sensing and communications: Toward dual-functional wireless networks for 6G and beyond," *IEEE J. Sel. Areas Commun.*, vol. 40, no. 6, pp. 1728–1767, Jun. 2022.

[20] H. S. Rou et al., "From orthogonal time–frequency space to affine frequency-division multiplexing: A comparative study of next-generation waveforms for integrated sensing and communications in doubly dispersive channels," *IEEE Signal Process. Mag.*, vol. 41, no. 5, pp. 71–86, Sep. 2024.

[21] A. Bemani, N. Ksairi, and M. Kountouris, "Affine frequency division multiplexing for next generation wireless communications," *IEEE Trans. Wireless Commun.*, vol. 22, no. 11, pp. 8214–8229, Nov. 2023.

[22] H. S. Rou, K. R. R. Ranasinghe, V. Savaux, G. T. F. de Abreu, D. González, and C. Masouros, "Affine frequency division multiplexing (AFDM) for 6G: Properties, features, and challenges," *IEEE Commun. Standards Mag.*, vol. 10, no. 2, pp. 216–225, Jun. 2026.

[23] Q. Li, J. Li, M. Wen, X. Dang, H. Arslan, and N. Al-Dhahir, "Affine frequency division multiplexing for 6G networks: Fundamentals, opportunities, and challenges," *IEEE Netw.*, vol. 40, no. 1, pp. 88–97, Jan. 2026.

[24] Y. Tao, M. Wen, Y. Ge, J. Li, E. Basar, and N. Al-Dhahir, "Affine frequency division multiplexing with index modulation: Full diversity condition, performance analysis, and low-complexity detection," *IEEE J. Sel. Areas Commun.*, vol. 43, no. 4, pp. 1041–1055, Apr. 2025.

[25] G. Liu et al., "Pre-chirp-domain index modulation for full-diversity affine frequency division multiplexing toward 6G," *IEEE Trans. Wireless Commun.*, vol. 24, no. 9, pp. 7331–7345, Sep. 2025.

[26] H. S. Rou et al., "AFDM chirp-permutation-index modulation with quantum-accelerated codebook design," in *Proc. 58th Asilomar Conf. Signal Syst. Comp.*, 2024, pp. 817–821.

[27] Y. Zhang, Q. Liu, Y. Ge, Y. Xu, C. Li, and Y. L. Guan, "Dual index modulation for affine frequency division multiplexing communications," *IEEE Wireless Commun. Lett.*, vol. 15, pp. 1469–1473, 2026.

[28] M. Qian, F. Ji, Y. Ge, M. Wen, and Y. Liang Guan, "Generalized code index modulation aided AFDM for spread spectrum systems," *IEEE Wireless Commun. Lett.*, vol. 14, no. 10, pp. 3229–3233, Oct. 2025.

[29] V. Savaux, H. S. Rou, Z. Sui, G. T. F. de Abreu, and Z. Liu, "On the robustness of AFDM and OTFS against passive eavesdroppers," *IEEE Wireless Commun. Lett.*, vol. 15, pp. 1365–1369, 2026.

[30] P. Wang et al., "A secure affine frequency division multiplexing for wireless communication systems," in *Proc. IEEE ICC*, Oct. 2025, pp. 2701–2706.

[31] H. S. Rou and G. T. F. de Abreu, "Chirp-permuted AFDM for quantum-resilient physical-layer secure communications," *IEEE Wireless Commun. Lett.*, vol. 14, no. 8, pp. 2376–2380, Aug. 2025.

[32] M. Ahmad, S. Baig, and N. A. Alqwaifly, "Radar-centric AFDM waveform with chirp-domain index modulation for ISAC," *IEEE Open J. Commun. Soc.*, vol. 7, pp. 844–857, 2026.

[33] Z. Sui et al., "Multi-functional chirp signalling for next-generation multi-carrier wireless networks: Communications, sensing and ISAC perspectives," 2025, *arXiv:2508.06022*.

[34] K. R. R. Ranasinghe et al., "Affine filter bank modulation (AFBM): A novel 6G ISAC waveform with low PAPR and OOBE," *IEEE Trans. Wireless Commun.*, vol. 25, pp. 12754–12769, 2026.

[35] Q. Yi, Z. Liu, L. Musavian, and Z. Sui, "Non-orthogonal affine frequency division multiplexing for spectrally efficient high-mobility communications," *IEEE Trans. Wireless Commun.*, vol. 25, pp. 15758–15774, 2026.

[36] H. L. Senger et al., "Affine filter bank modulation: A new waveform for high mobility communications," 2025, *arXiv:2505.03589*.

[37] Z. Wei et al., "Orthogonal time-frequency space modulation: A promising next-generation waveform," *IEEE Wireless Commun.*, vol. 28, no. 4, pp. 136–144, Aug. 2021.

[38] Z. Sui et al., "Performance analysis and approximate message passing detection of orthogonal time sequency multiplexing modulation," *IEEE Trans. Wireless Commun.*, vol. 23, no. 3, pp. 1913–1928, Mar. 2024.

[39] H. Lin and J. Yuan, "Orthogonal delay-Doppler division multiplexing modulation," *IEEE Trans. Wireless Commun.*, vol. 21, no. 12, pp. 11024–11037, Dec. 2022.

[40] F. Lampel, A. Avarado, and F. M. J. Willems, "On OTFS using the discrete zak transform," in *Proc. IEEE Int. Conf. Commun. Workshops (ICC Workshops)*, May 2022, pp. 729–734.

[41] Y. Hong, T. Thaj, and E. Viterbo, *Delay-Doppler Communications: Principles and Applications*. New York, NY, USA: Academic, 2022.

[42] Q. Deng, Y. Ge, and Z. Ding, "A unifying view of OTFS and its many variants," *IEEE Commun. Surveys Tuts.*, vol. 27, no. 6, pp. 3561–3586, Dec. 2025.

[43] S. Li, J. Yuan, W. Yuan, Z. Wei, B. Bai, and D. W. K. Ng, "Performance analysis of coded OTFS systems over high-mobility channels," *IEEE Trans. Wireless Commun.*, vol. 20, no. 9, pp. 6033–6048, Sep. 2021.

[44] G. D. Surabhi, R. M. Augustine, and A. Chockalingam, "On the diversity of uncoded OTFS modulation in doubly-dispersive channels," *IEEE Trans. Wireless Commun.*, vol. 18, no. 6, pp. 3049–3063, Jun. 2019.

[45] A. Bemani, G. Cuozzo, N. Ksairi, and M. Kountouris, "Affine frequency division multiplexing for next-generation wireless networks," in *Proc. 17th Int. Symp. Wireless Commun. Syst. (ISWCS)*, Sep. 2021, pp. 1–6.

[46] A. Bemani, N. Ksairi, and M. Kountouris, "Integrated sensing and communications with affine frequency division multiplexing (AFDM)," *IEEE Wireless Commun. Lett.*, vol. 13, no. 5, pp. 1255–1259, May 2024.

[47] Y. Luo, Y. L. Guan, Y. Ge, and C. Yuen, "Target sensing with off-grid sparse Bayesian learning for AFDM-ISAC system," in *Proc. IEEE Int. Conf. Commun. Workshops (ICC Workshops)*, Jun. 2025, pp. 881–886.

[48] Y. Ni, P. Yuan, Q. Huang, F. Liu, and Z. Wang, "An integrated sensing and communications system based on affine frequency division multiplexing," *IEEE Trans. Wireless Commun.*, vol. 24, no. 5, pp. 3763–3779, May 2025.

[49] Y. Luo, Y. L. Guan, Y. Ge, D. González G, and C. Yuen, "A novel angle-delay-Doppler estimation scheme for AFDM-ISAC system in mixed near-field and far-field scenarios," *IEEE Internet Things J.*, vol. 12, no. 13, pp. 22669–22682, Jul. 2025.

[50] H. S. Rou and G. T. F. De Abreu, "Normalized ambiguity function characteristics of OFDM, OTFS, AFDM, and CP-AFDM for ISAC," in *Proc. IEEE Int. Conf. Commun.*, May 2026, pp. 1–6.

[51] Y. Ni, F. Liu, H. Yin, Y. Tang, Y. Ma, and Z. Wang, "Ambiguity function analysis of AFDM under pulse-shaped random ISAC signaling," *IEEE Trans. Wireless Commun.*, vol. 25, pp. 13619–13635, 2026.

[52] J. Zhu, Y. Tang, F. Liu, X. Zhang, H. Yin, and Y. Zhou, "AFDM-based bistatic integrated sensing and communication in static scatterer environments," *IEEE Wireless Commun. Lett.*, vol. 13, no. 8, pp. 2245–2249, Aug. 2024.

[53] F. Zhang et al., "AFDM-enabled integrated sensing and communication: Theoretical framework and pilot design," *IEEE J. Sel. Areas Commun.*, vol. 44, pp. 310–324, 2026.

[54] K. Ramadan, A. A. Alharbi, and E. S. Hassan, "Performance evaluation of AFDM for integrated sensing and communications in doubly dispersive channels," *Defence Technol.*, vol. 61, pp. 110–125, Jul. 2026.

[55] X. Ouyang and J. Zhao, "Orthogonal chirp division multiplexing," *IEEE Trans. Commun.*, vol. 64, no. 9, pp. 3946–3957, Sep. 2016.

[56] K. R. R. Ranasinghe, Z. Wang, H. S. Rou, G. T. F. de Abreu, and E. Björnson, "Doubly-dispersive continuous MIMO systems: Channel modeling and beamforming design," *IEEE Trans. Wireless Commun.*, vol. 25, pp. 15441–15458, 2026.

[57] K. R. R. Ranasinghe, I. A. M. Sandoval, H. S. Rou, G. T. F. de Abreu, and G. C. Alexandropoulos, "Doubly-dispersive MIMO channels with stacked intelligent metasurfaces: Modeling, parametrization, and receiver design," *IEEE Trans. Wireless Commun.*, vol. 25, pp. 3801–3817, 2026.

[58] K. R. R. Ranasinghe et al., "Flexible intelligent metasurfaces in high-mobility MIMO integrated sensing and communications," *IEEE Trans. Wireless Commun.*, vol. 25, pp. 13319–13335, 2026.

[59] Y. Chi, Z. Peng, L. Liu, Y. Li, Y. Ge, and C. Yuen, "Achievable rate and coding principle for MIMO multicarrier systems with cross-domain MAMP receiver over doubly selective channels," *IEEE Trans. Wireless Commun.*, vol. 25, pp. 10354–10370, 2026.

[60] R. W. Bäuml, R. F. H. Fischer, and J. B. Huber, "Reducing the peak-to-average power ratio of multicarrier modulation by selected mapping," *Electron. Lett.*, vol. 32, no. 22, pp. 2056–2057, Oct. 1996.

[61] *Evolved Universal Terrestrial Radio Access (E-UTRA); Physical Channels and Modulation*, document TS 36.211 V17.2.0, 3GPP, 2022.

[62] Wireless LAN Medium Access Control (MAC) and Physical Layer (PHY) Specifications, IEEE Standard 802.11-2012, 2012.

[63] Digital Video Broadcasting (DVB); Framing Structure, Channel Coding and Modulation for Digital Terrestrial Television, Standard ETSI EN 300 744 V1.6.1, 2009.

[64] H. Yin, Y. Tang, S. Li, Y. Zhou, and C. Yi, "Evaluation and design criterion for pulse-shaped AFDM," in *Proc. IEEE Global Commun. Conf.*, Dec. 2024, pp. 4944–4949.

[65] M. Mirabella, P. Di Viesti, and G. M. Vitetta, "On the use of a two-dimensional cyclic prefix in OTFS modulation and its implications," *IEEE Open J. Commun. Soc.*, vol. 5, pp. 3340–3367, 2024.

[66] H. Yin and Y. Tang, "Pilot aided channel estimation for AFDM in doubly dispersive channels," in *Proc. IEEE/CIC Int. Conf. Commun. China (ICCC)*, Aug. 2022, pp. 308–313.

[67] Y. Zhou, H. Yin, N. Zhou, Y. Tang, X. Zhang, and W. Yuan, "GI-free pilot-aided channel estimation for affine frequency division multiplexing systems," 2024, *arXiv:2404.01088*.

[68] K. Zheng, M. Wen, T. Mao, L. Xiao, and Z. Wang, "Channel estimation for AFDM with superimposed pilots," *IEEE Trans. Veh. Technol.*, vol. 74, no. 2, pp. 3389–3394, Feb. 2025.

[69] V. Savaux, "Pilot design for multiple domains channel estimation in special cases of affine frequency division multiplexing," *Phys. Commun.*, vol. 73, Dec. 2025, Art. no. 102863.

[70] V. Savaux, "Special cases of DFT-based modulation and demodulation for affine frequency division multiplexing," *IEEE Trans. Commun.*, vol. 72, no. 12, pp. 7627–7638, Dec. 2024.

[71] *NR; Physical Channels and Modulation*, 3GPP, document TS 38.211 v16.2.0, Jul. 2020.

[72] V. Savaux and Y. Louët, "LMMSE channel estimation in OFDM context: A review," *IET Signal Process.*, vol. 11, no. 2, pp. 123–134, Apr. 2017.

[73] X. Li et al., "Low-complexity channel estimation for Internet of Vehicles AFDM communications with sparse Bayesian learning," *IEEE Internet Things J.*, vol. 13, no. 5, pp. 9795–9810, Mar. 2026.

[74] C. Shen, J. Yuan, and J. Tong, "Time-domain zero-padding (TZP) AFDM with two-stage iterative MMSE detection," *IEEE Trans. Wireless Commun.*, vol. 25, pp. 6255–6269, 2026.

[75] H. Hawkins, C. Xu, L.-L. Yang, and L. Hanzo, "Iterative soft-MMSE detection aided AFDM and OTFS," *IEEE Open J. Veh. Technol.*, vol. 6, pp. 2944–2959, 2025.

[76] Z. Sui, Z. Liu, L. Musavian, L.-L. Yang, and L. Hanzo, "Generalized spatial modulation aided affine frequency division multiplexing," *IEEE Trans. Wireless Commun.*, vol. 25, pp. 4658–4673, 2026.

[77] Z. Li, C. Zhang, G. Song, X. Fang, X. Sha, and D. T. M. Slock, "Chirp parameter selection for affine frequency division multiplexing with MMSE equalization," *IEEE Trans. Commun.*, vol. 73, no. 7, pp. 5079–5093, Jul. 2025.

[78] S. Tiwari, S. S. Das, and V. Rangamgari, "Low complexity LMMSE receiver for OTFS," *IEEE Commun. Lett.*, vol. 23, no. 12, pp. 2205–2209, Dec. 2019.

[79] Q. Yi, Z. Sui, and Z. Liu, "Error rate analysis and low-complexity receiver design for zero-padded AFDM," *IEEE Trans. Veh. Technol.*, early access, Apr. 30, 2026, doi: 10.1109/TVT.2026.3689279.

[80] A. Bemani, N. Ksairi, and M. Kountouris, "Low complexity equalization for afdm in doubly dispersive channels," in *Proc. IEEE Int. Conf. Acoust., Speech Signal Process. (ICASSP)*, May 2022, pp. 5273–5277.

[81] Q. Luo et al., "AFDM-SCMA: A promising waveform for massive connectivity over high mobility channels," *IEEE Trans. Wireless Commun.*, vol. 23, no. 10, pp. 14421–14436, Oct. 2024.

[82] X. Li et al., "Affine frequency division multiplexing over wideband doubly-dispersive channels with time-scaling effects," *IEEE Trans. Wireless Commun.*, vol. 25, pp. 476–492, 2026.

[83] K. R. R. Ranasinghe, H. S. Rou, G. T. F. de Abreu, T. Takahashi, and K. Ito, "Joint channel, data, and radar parameter estimation for AFDM systems in doubly-dispersive channels," *IEEE Trans. Wireless Commun.*, vol. 24, no. 2, pp. 1602–1619, Feb. 2025.

[84] Y. Xu, L. Xiao, C. Ding, P. Xiao, M. Wen, and T. Jiang, "AFDM-aided grant-free random access for LEO SIoT: Performance analysis and near-optimal joint detection," *IEEE Trans. Commun.*, vol. 74, pp. 840–853, 2026.

[85] Q. Luo et al., "Joint sparse graph for enhanced MIMO-AFDM receiver design," *IEEE Trans. Wireless Commun.*, vol. 25, pp. 3272–3286, 2026.

[86] M. Tuchler, A. C. Singer, and R. Koetter, "Minimum mean squared error equalization using a priori information," *IEEE Trans. Signal Process.*, vol. 50, no. 3, pp. 673–683, Mar. 2002.

[87] H. Yin, X. Wei, Y. Tang, and K. Yang, "Diagonally reconstructed channel estimation for MIMO-AFDM with inter-Doppler interference in doubly selective channels," *IEEE Trans. Wireless Commun.*, vol. 23, no. 10, pp. 14066–14079, Oct. 2024.

[88] V. Savaux and X. Chen, "Spatial precoding in frequency domain for multi-user MIMO affine frequency division multiplexing," in *Proc. 32nd Eur. Signal Process. Conf. (EUSIPCO)*, Aug. 2024, pp. 2112–2116.

[89] R. Y. Bir, A. Ammar Boudjelal, and H. Arslan, "On the orthogonal coexistence of AFDM and OFDM for joint sensing and communication," *IEEE Open J. Commun. Soc.*, vol. 6, pp. 10010–10022, 2025.

[90] K. Abela, S. Abidrabbu, A. Ammar Boudjelal, and H. Arslan, "A SIC-free dual-domain RSMA strategy via AFDM–OFDM coexistence for 6G networks," *IEEE Trans. Commun.*, vol. 74, pp. 11315–11325, 2026.

[91] Y. Yin, Z. Zhang, X. Yang, Y. Gong, and L. Wang, "Downlink AFDM-RSMA scheme based on orthogonal chirps and sum-rate maximization," in *Proc. IEEE/CIC Int. Conf. Commun. China (ICCC)*, Aug. 2025, pp. 1–6.

[92] H. Liu, Q. Luo, Z. Liu, S. Luo, P. Xiao, and R. Lin, "BER analysis of SCMA-OFDM systems in the presence of carrier frequency offset," *IEEE Commun. Lett.*, vol. 28, no. 1, pp. 213–217, Jan. 2024.

[93] Y. Tao, M. Wen, Y. Ge, T. Mao, Y. Tang, and A. Doosti-Aref, "Affine frequency division multiple access based on DAFT spreading for next-generation wireless networks," *IEEE Trans. Wireless Commun.*, vol. 25, pp. 4626–4641, 2026.

[94] L. Piazzo and P. Mandarini, "Analysis of phase noise effects in OFDM modems," *IEEE Trans. Commun.*, vol. 50, no. 10, pp. 1696–1705, Oct. 2002.

[95] Z. Sui, Z. Liu, L. Musavian, Y. L. Guan, L.-L. Yang, and L. Hanzo, "MIMO-AFDM outperforms MIMO-OFDM in the face of hardware impairments," *IEEE Trans. Commun.*, vol. 74, pp. 10432–10447, 2026.

[96] D. D. Lin and T. J. Lim, "The variational inference approach to joint data detection and phase noise estimation in OFDM," *IEEE Trans. Signal Process.*, vol. 55, no. 5, pp. 1862–1874, May 2007.

[97] Z. Sui, H. Q. Ngo, M. Matthaiou, and L. Hanzo, "Performance analysis and optimization of STAR-RIS-aided cell-free massive MIMO systems relying on imperfect hardware," *IEEE Trans. Wireless Commun.*, vol. 24, no. 4, pp. 2925–2939, Apr. 2025.

[98] E. Björnson, M. Matthaiou, and M. Debbah, "Massive MIMO with non-ideal arbitrary arrays: Hardware scaling laws and circuit-aware design," *IEEE Trans. Wireless Commun.*, vol. 14, no. 8, pp. 4353–4368, Aug. 2015.

[99] E. Basar, Ü. Aygölü, E. Panayirci, and H. V. Poor, "Orthogonal frequency division multiplexing with index modulation," *IEEE Trans. Signal Process.*, vol. 61, no. 22, pp. 5536–5549, Nov. 2013.

[100] Z. Sui, S. Yan, H. Zhang, L.-L. Yang, and L. Hanzo, "Approximate message passing algorithms for low complexity OFDM-IM detection," *IEEE Trans. Veh. Technol.*, vol. 70, no. 9, pp. 9607–9612, Sep. 2021.

[101] Y. Tao, M. Wen, Y. Ge, and J. Li, "Affine frequency division multiplexing with index modulation," in *Proc. IEEE Wireless Commun. Netw. Conf. (WCNC)*, Apr. 2024, pp. 1–6.

[102] R. Y. Mesleh et al., "Spatial modulation," *IEEE Trans. Veh. Technol.*, vol. 57, no. 4, pp. 2228–2241, Jul. 2008.

[103] H. S. Rou, G. T. F. de Abreu, H. Iimori, and O. Gonsa, "Scalable quadrature spatial modulation," *IEEE Trans. Wireless Commun.*, vol. 21, no. 11, pp. 9293–9311, Nov. 2022.

[104] Z. Sui, H. Zhang, Y. Xin, T. Bao, L.-L. Yang, and L. Hanzo, "Low complexity detection of spatial modulation aided OTFS in doubly-selective channels," *IEEE Trans. Veh. Technol.*, vol. 72, no. 10, pp. 13746–13751, Oct. 2023.

[105] Z. Sui, H. Zhang, S. Sun, L.-L. Yang, and L. Hanzo, "Space-time shift keying aided OTFS modulation for orthogonal multiple access," *IEEE Trans. Commun.*, vol. 71, no. 12, pp. 7393–7408, Dec. 2023.
[106] J. Zhu, Q. Luo, G. Chen, P. Xiao, and L. Xiao, "Design and performance analysis of index modulation empowered AFDM system," *IEEE Wireless Commun. Lett.*, vol. 13, no. 3, pp. 686–690, Mar. 2024.
[107] M. Temiz and C. Masouros, "Affine frequency division multiplexing with subcarrier power-level index modulation for integrated sensing and communications," in *Proc. IEEE 26th Int. Workshop Signal Process. Artif. Intell. Wireless Commun. (SPAWC)*, Jul. 2025, pp. 1–5.
[108] A. Anoop, C. K. Thomas, S. Kala, J. V. B. Benifa, and W. Saad, "Dual-mode index modulation based on affine frequency division multiplexing," *Phys. Commun.*, vol. 70, Jun. 2025, Art. no. 102628.
[109] G. Liu, T. Mao, Y. Tang, J. Zhao, Z. Xiao, and Z. Han, "Multiple-mode affine frequency division multiplexing with index modulation," *IEEE Wireless Commun. Lett.*, vol. 15, pp. 141–145, 2026.
[110] H. Seok Rou and G. Thadeu Freitas de Abreu, "Chirp-permuted AFDM: A versatile waveform design for ISAC in 6G," 2025, *arXiv:2507.20825*.
[111] V. Savaux, S. Sawadogo, H. S. Rou, and G. T. F. de Abreu, "On the noise robustness of affine frequency division multiplexing: Analysis and applications," in *Proc. 4th Int. Conf. 6G Netw. (6GNet)*, Dec. 2025, pp. 65–72.
[112] V. M. Reddy and H. Bitra, "PAPR in AFDM: Upper bound and reduction with normalized μ-law companding," *IEEE Access*, vol. 13, pp. 86553–86561, 2025.
[113] A. Ali, A. Arous, and H. Arslan, "Spreading the wave: Low-complexity PAPR reduction for AFDM and OCDM in 6G networks," *IEEE Trans. Green Commun. Netw.*, vol. 10, pp. 1565–1577, 2026.
[114] H. Yuan et al., "PAPR reduction with pre-chirp selection for affine frequency division multiplexing," *IEEE Wireless Commun. Lett.*, vol. 14, no. 3, pp. 736–740, Mar. 2025.
[115] Z. Lu, M. El-Hajjar, and L.-L. Yang, "Augmented affine frequency division multiplexing for low PAPR signaling and diversity gain protection," *IEEE Access*, vol. 14, pp. 69426–69442, 2026.
[116] G. D. Surabhi, M. Kollengode Ramachandran, and A. Chockalingam, "OTFS modulation with phase noise in mmWave communications," in *Proc. IEEE 89th Veh. Technol. Conf. (VTC-Spring)*, Kuala Lumpur, Malaysia, Apr. 2019, pp. 1–5.
[117] A. Abushattal, S. E. Zegrar, A. Yazgan, and H. Arslan, "A comprehensive experimental emulation for OTFS waveform RF-impairments," *Sensors*, vol. 23, no. 1, p. 38, Dec. 2022.



HYEON SEOK ROU (Member, IEEE) received the B.Sc. degree in electrical and computer engineering and the Ph.D. degree in electrical engineering from Constructor University Bremen (formerly Jacobs University Bremen), Germany, in 2021 and 2024, respectively. Since 2025, he has been a Post-Doctoral Research Fellow and a Lecturer with the School of Computer Science and Engineering, Constructor University Bremen. In November 2026, he will join the School of Electrical Engineering, Korea Advanced Institute of Science and Technology (KAIST), Daejeon, South Korea, as a Research Assistant Professor. His research interests include next-generation (B5G and 6G) wireless systems, affine frequency division multiplexing (AFDM), integrated sensing and communications (ISAC), high-mobility communications, multi-dimensional sparse modulation, over-the-air computing (AirComp), vehicle-to-everything (V2X) communications, and quantum-accelerated optimization. In 2026, he was selected as a Brain Pool Fellow by the National Research Foundation of Korea (NRF). He has been a Chapter Representative of Korean Scientists and Engineers Association in the Federal Republic of Germany (VeKNI e.V.) since 2021. He was the German delegate to theYoung Professionals Forum (YPF) of the third World Congress of Korean Scientists and Engineers, South Korea, in 2025. In 2023, he was a Visiting Researcher with the Intelligent Communications Systems Laboratory (ICL), KAIST. In 2022, he received Korea Institute of Science and Technology Europe Research Scholarship Award. He also contributes to the IEEE Standards Association P3383 Working Group on Performance Metrics for Integrated Sensing and Communication.



VINCENT SAVAUX (Senior Member, IEEE) received the Engineering degree from the High School of Engineering, ECAM Rennes, the M.Sc. degree from the University of Rennes 1, France, in 2010, and the Ph.D. degree in telecommunications from École Supérieure d'Électricité-Supélec in 2013. From 2014 to 2015, he was a Post-Doctoral Researcher with CentraleSupélec, Campus de Rennes, France. Since 2016, he has been a Research Engineer with the Institute of Research and Technology b-com, Rennes, France. His research activities mainly focus on signal processing for wireless systems, including the IoT technologies, MIMO systems, physical layer security, and new waveforms for next generations of communications systems. He has published more than 70 papers in high-level international journals and conferences and he serves as a TPC member for several conferences. He received the Exemplary Reviewer 2014 Appreciation from IEEE WIRELESS COMMUNICATIONS LETTERS and IEEE COMMUNICATIONS LETTERS, and the Best Paper Award from IEEE CSCN 2023.



ZEPING SUI (Member, IEEE) received the Ph.D. degree in signal and information processing from the University of Chinese Academy of Sciences, Beijing, China, in 2023. From March 2022 to February 2023, he was a Research Assistant with the Institute for Infocomm Research (I2R), Agency for Science, Technology and Research (A*STAR), Singapore. From August 2023 to August 2024, he was a Research Fellow with the Centre for Wireless Innovation (CWI), Queen's University Belfast, Belfast, U.K. He is currently a Senior Research Officer with the School of Computer Science and Electronic Engineering (CSEE), University of Essex, Colchester, U.K. His research interests span signal processing for wireless communications, waveform design, hardware-constrained communication systems, statistical signal processing, and beyond massive MIMO. He received the Exemplary Reviewer Award from IEEE WIRELESS COMMUNICATIONS LETTERS in 2025. He has served as an Organizer/Chair of several workshops and special sessions at flagship IEEE conferences, including IEEE GLOBECOM, IEEE PIMRC, IEEE WCNC, IEEE/CIC ICCC, IEEE Ucom, and IEEE SPAWC, and a Tutorial Speaker for IEEE WCNC 2026. He also serves as an Editor for IEEE TRANSACTIONS ON COMMUNICATIONS, an Associate Editor for IEEE WIRELESS COMMUNICATIONS LETTERS, and a Senior Reviewer for IEEE OPEN JOURNAL OF THE COMMUNICATIONS SOCIETY.



GIUSEPPE THADEU FREITAS DE ABREU (Senior Member, IEEE) received the B.Eng. degree in electrical engineering and the specialization Lato Sensu degree in telecommunications engineering from the Universidade Federal da Bahia (UFBa), Salvador, Bahia, Brazil, in 1996 and 1997, respectively, and the M.Eng. and D.Eng. degrees in physics, electrical, and computer engineering from Yokohama National University, Japan, in March 2001 and March 2004, respectively. He was a Post-Doctoral Fellow and later an Adjunct Professor (Docent) in statistical signal processing and communications theory with the Department of Electrical and Information Engineering, University of Oulu, Finland, from 2004 to 2006 and from 2006 to 2011, respectively. Since 2011, he has been a Professor in electrical engineering with Constructor University Bremen (formerly Jacobs University), Bremen, Germany. From April 2015 to August 2018, he simultaneously held a full tenured professorship also with the Department of Computer and Electrical Engineering, Ritsumeikan University, Japan. He has been a Visiting Scholar at Rice University in 2008, Stanford University in 2009, Keio University in 2010, the University of Bologna in 2012 and 2014, and KTH Royal Institute of Technology in 2025. He has also been a Regular Visiting Professor with The University of Electro-Communications, Japan, since 2013. He has been a Visiting Scholar with Stanford University, Rice University, York University, ETH Zürich, over the years. He was a Scholar in Residence with KTH Royal Institute of Technology, Sweden, from September 2025 to January 2026. He received Uenohara Award at Tokyo University in 2000 for his master's thesis work. He was a co-recipient of awards from various international IEEE conferences, including the Asilomar in 2009, 2012, and 2014, WPNC in 2012 and 2015, ISWCS in 2016, WPMC in 2023, and ICNC in 2025. He was also a co-recipient of the Best Journal Paper Award by Japanese Chapter of the IEEE Signal Processing Society in 2023. He was awarded various prestigious fellowships from Heiwa Nakajima Foundation, Japanese Society for the Promotion of Science (JSPS), and twice from the National Institute for Communications Technologies (NICT), respectively, in 2010, 2013, 2015, and 2018. He served as an Editor for various IEEE journals, including IEEE TRANSACTIONS ON WIRELESS COMMUNICATIONS, IEEE TRANSACTIONS ON COMMUNICATIONS, IEEE COMMUNICATIONS LETTERS, IEEE SIGNAL PROCESSING LETTERS, and IEEE OPEN JOURNAL OF THE COMMUNICATIONS SOCIETY. He was also the Executive Editor for IEEE TRANSACTIONS ON WIRELESS COMMUNICATIONS from 2017 to 2021. Since 2026,he has been the Editor-at-Large for Wireless Communications of IEEE OPEN JOURNAL OF THE COMMUNICATIONS SOCIETY. His research interests span a wide range of topics on wireless communications and signal processing, including communications theory, estimation theory, optimization theory, statistical modeling, metasurfaces and electromagnetic structures, waveform design, integrated sensing and communications, over-the-air computing, wireless localization, cognitive radio, wireless security, MIMO systems, ultrawideband and millimeter wave communications, full-duplex and cognitive radio, compressive sensing, energy harvesting networks, random networks, and connected vehicles networks.

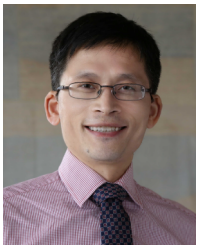

ZILONG LIU (Senior Member, IEEE) received the bachelor's degree from Huazhong University of Science and Technology in 2004, the M.Sc. degree from Tsinghua University in 2007, and the Ph.D. degree from Nanyang Technological University, Singapore, in 2017. He is currently an Associate Professor, the 6G Laboratory Manager, and the 2024 Outstanding Mid-Career Researcher with the Faculty of Science and Health, University of Essex, Colchester, U.K. He was a Visiting Ph.D. Student with The University of Melbourne in 2012, a Visiting Ph.D. Student with The Hong Kong University of Science and Technology in 2012, and a Senior Research Fellow with the University of Surrey (2018–2019). He is/was a Distinguished Lecturer of the IEEE Vehicular Technology Society, a recipient of the prestigious EPSRC New Investigator Award (NIA), U.K., and a Consultant to the National Institute of Information and Communication Technology (NICT), a Japanese Government organization, on 6G V2X assisted autonomous driving. His research generally lies in the interplay of coding, signal processing, and communications, with a major objective of bridging theory and practice. At Essex, he has led the successful development of real-time over-the-air USRP testbeds of OFDM-SCMA and AFDM, which were demonstrated at MWC'2026 and ICC'2026, respectively. He has widely published in quality journals, such as IEEE TRANSACTIONS ON INFORMATION THEORY, IEEE TRANSACTIONS ON SIGNAL PROCESSING, IEEE JOURNAL ON SELECTED AREAS IN COMMUNICATIONS, IEEE JOURNAL OF SELECTED TOPICS IN SIGNAL PROCESSING, and *Proceedings of the IEEE*. He has made a series of original contributions to waveforms, sequences, and multiple access. He is/was the Hosting General Chair of IWSDA'2022 (iwsda2022.github.io) and SETA'2024 (seta-2024.github.io), an active contributor to flagship IEEE conferences (e.g., GLOBECOM'2026, PIMRC'2026, ISIT'2026, ICC'2026, ICCC'2026, WCNC'2026, VTC-Fall'2025, and IWSDA'2025) in various roles (e.g., the track co-chair, a tutorial/keynote speaker, a workshop organizer, and a TPC member), and an Associate Editor for several leading IEEE journals, including IEEE TRANSACTIONS ON WIRELESS COMMUNICATIONS, IEEE TRANSACTIONS ON VEHICULAR TECHNOLOGY, IEEE WIRELESS COMMUNICATIONS LETTERS, and IEEE OPEN JOURNAL OF THE COMMUNICATIONS SOCIETY. For more information visit the link https://sites.google.com/site/zilongliu2357